A synthesis of marine sediment core ^{13}C data over the last 150 000 years

Clim. Past, 6, 645–673, 2010
www.clim-past.net/6/645/2010/
doi:10.5194/cp-6-645-2010

Climate of the Past

A synthesis of marine sediment core δ^{13}C data over the last 150 000 years

K. I. C. Oliver[1,2], **B. A. A. Hoogakker**[3], **S. Crowhurst**[3], **G. M. Henderson**[4], **R. E. M. Rickaby**[4], **N. R. Edwards**[2], **and H. Elderfield**[3]

[1]School of Ocean and Earth Science, National Oceanography Centre Southampton, University of Southampton, European Way, Southampton SO14 3ZH, UK
[2]Department of Earth and Environmental Sciences, The Open University, Walton Hall, Milton Keynes MK7 6AA, UK
[3]Department of Earth Sciences, University of Cambridge, Downing Street, Cambridge CB2 2EQ, UK
[4]Department of Earth Sciences, University of Oxford, Parks Road, Oxford OX1 3PR, UK

Received: 19 November 2009 – Published in Clim. Past Discuss.: 11 December 2009
Revised: 6 September 2010 – Accepted: 7 September 2010 – Published: 8 October 2010

Abstract. The isotopic composition of carbon, δ^{13}C, in seawater is used in reconstructions of ocean circulation, marine productivity, air-sea gas exchange, and biosphere carbon storage. Here, a synthesis of δ^{13}C measurements taken from foraminifera in marine sediment cores over the last 150 000 years is presented. The dataset comprises previously published and unpublished data from benthic and planktonic records throughout the global ocean. Data are placed on a common δ^{18}O age scale suitable for examining orbital timescale variability but not millennial events, which are removed by a 10 ka filter. Error estimates account for the resolution and scatter of the original data, and uncertainty in the relationship between δ^{13}C of calcite and of dissolved inorganic carbon (DIC) in seawater. This will assist comparison with δ^{13}C of DIC output from models, which can be further improved using model outputs such as temperature, DIC concentration, and alkalinity to improve estimates of fractionation during calcite formation.

High global deep ocean δ^{13}C, indicating isotopically heavy carbon, is obtained during Marine Isotope Stages (MIS) 1, 3, 5a, c and e, and low δ^{13}C during MIS 2, 4 and 6, which are temperature minima, with larger amplitude variability in the Atlantic Ocean than the Pacific Ocean. This is likely to result from changes in biosphere carbon storage, modulated by changes in ocean circulation, productivity, and air-sea gas exchange. The North Atlantic vertical δ^{13}C gradient is greater during temperature minima than temperature maxima, attributed to changes in the spatial extent of Atlantic source waters. There are insufficient data from shallower than 2500 m to obtain a coherent pattern in other ocean basins. The data synthesis indicates that basin-scale δ^{13}C during the last interglacial (MIS 5e) is not clearly distinguishable from the Holocene (MIS 1) or from MIS 5a and 5c, despite significant differences in ice volume and atmospheric CO_2 concentration during these intervals. Similarly, MIS 6 is only distinguishable from MIS 2 or 4 due to globally lower δ^{13}C values both in benthic and planktonic data. This result is obtained despite individual records showing differences between these intervals, indicating that care must be used in interpreting large scale signals from a small number of records.

Correspondence to: K. I. C. Oliver
(k.oliver@noc.soton.ac.uk)

1 Introduction

The isotopic composition, δ^{13}C, of inorganic carbon in seawater is a diagnostic of ocean circulation and the marine and terrestrial carbon cycle. The potential for δ^{13}C in calcium carbonate shells, formed by foraminifera and preserved in marine sediments, to record past changes in climate has been recognised since the 1970s (Shackleton, 1977; Duplessy et al., 1981a). Greater differences in δ^{13}C between planktonic and benthic foraminifera, during glacial periods, were interpreted as indicating greater storage of isotopically light organic carbon in the deep ocean and linked to atmospheric pCO_2 (Broecker, 1982a; Shackleton et al., 1983; Shackleton et al., 1992). Lower δ^{13}C values recorded in the Pacific Ocean, during the last glacial maximum (LGM), were attributed to a change in the ocean δ^{13}C reservoir due to the release of organic carbon from the terrestrial biosphere or marine shelf sediments (Broecker, 1982b; Duplessy et al., 1988b). Carbon isotopes have also been used to reconstruct past water masses, notably low δ^{13}C Antarctic

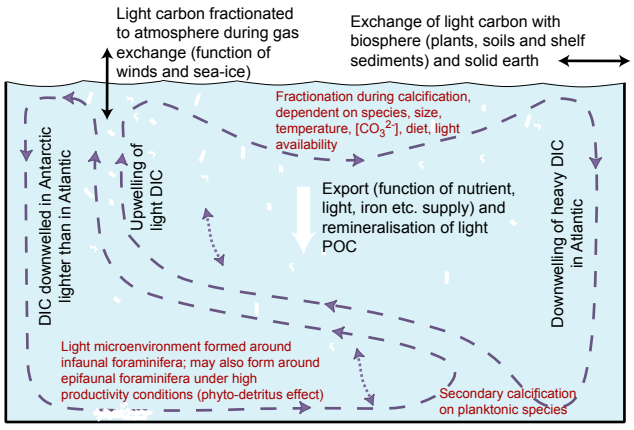

Fig. 1. Schematic of processes influencing δ^{13}C recorded in calcium carbonate from foraminiferal shells. Processes in large font affect δ^{13}C of dissolved inorganic carbon (DIC) in open seawater; processes in small font affect the difference between recorded δ^{13}C and seawater δ^{13}C. POC ≡ particulate organic carbon. Heavy (light) DIC refers to DIC rich (poor) in ^{13}C.

source waters and high δ^{13}C Atlantic source waters (Sarnthein et al., 1994), or to diagnose changes in air-sea gas exchange (Marchitto and Broecker, 2006). However, the interpretation of the δ^{13}C is complicated by the dependence of fractionation during calcification on properties of the water (temperature; $[CO_2]$; $[CO_3^{2-}]$) and the foraminifer (species; shell size; diet), and on the formation of microenvironments around benthic foraminifera (Sect. 3). The variety of mechanisms influencing the δ^{13}C record is summarised in Fig. 1.

The reconstruction of past ocean states depends on the collation of δ^{13}C observations from throughout the ocean, which can provide a fairer test to hypotheses than individual datasets. The demand for such syntheses is increased by the development of Earth system models that are able to simulate paleoclimate proxies including δ^{13}C (Ridgwell et al., 2007; Brovkin et al., 2007). Previous data syntheses have consisted of time-slices for selected regions such as the Atlantic Ocean (Sarnthein et al., 1994; Bickert and Mackensen, 2003; Curry and Oppo, 2005; Lynch-Stieglitz et al., 2007), typically focusing on the difference between the late Holocene and the LGM. Data from the benthic species *Cibicidoides wuellerstorfi*, considered the most reliable indicator of seawater δ^{13}C, were selected for those time-slices, reducing the error in the data at the expense of reduced data coverage. In this study, we focus not on specific time-slices but on producing a synthesis of time-slices for the last 150 ka. We include data from a range of benthic and planktonic species, and do not exclude data from high productivity regions. The inhomogeneity in this data is addressed by attaching an error estimate for each observation, using the entire dataset to estimate additional errors associated with less reliable species and unfavourable core locations.

The goals for this study are threefold: (1) to provide a common δ^{18}O-derived age-scale for a synthesis of δ^{13}C data; (2) to provide δ^{13}C error estimates for the synthesis, in order to facilitate direct model–data comparison; (3) to provide a global overview of the data, and an account of the large scale processes invoked to explain changes in ocean δ^{13}C. In Sect. 2, we introduce the data and the age-scale. In Sect. 3, we describe the methods used to determine uniformly spaced time-series and uncertainty intervals. In Sect. 4, we examine δ^{13}C time-series, grouped by region, and time-slices, as well as planktonic-benthic differences. We summarise our findings in Sect. 5, and discuss their application for Earth System models and biosphere reconstructions.

2 Data

2.1 Data selection and coverage

Table 1 summarises the data used in this compilation. Data consist mostly of records submitted to the PANGAEA publishing network for geoscientific and environmental data (http://pangaea.de), the National Geophysical Data Centre (NGDC; http://www.ngdc.noaa.gov), or the Delphi Project (http://www.esc.cam.ac.uk/research/research-groups/delphi), with additional records obtained through personal correspondence. δ^{13}C records were accepted into the pre-processed compilation provided that it was possible to obtain a reliable (though sometimes low resolution) age model within the last 150 000 years using δ^{18}O stratigraphy. No data quality constraint was applied to the pre-processed compilation, but several factors (detailed in Sect. 3) can lead to a large error estimate. Where the cumulative errors exceeded 1‰, data were rejected as having too large an error to be useful. Entire records rejected by this process are flagged in Table 1.

Figure 2 shows the core locations for the records used in the data synthesis, as well as for records for which we were unable to provide a δ^{18}O–derived age model. Among the records that were used, there is good data coverage in deep waters (>2500 m) in the Atlantic Ocean (100 cores with benthic data). Atlantic data coverage is also reasonable at shallower depths (45 cores) and in surface waters (71 cores with planktonic data). The principal gaps in benthic data coverage are: (1) <2500 m in the Pacific ocean (10 cores); (2) the Indian ocean (12 cores); and (4) south of 50° S (2 cores). There is a large variation in the temporal resolution of the pre-processed data, both within and across cores. Of the cores providing benthic data, all but 28 provide at least one observation for the LGM (19–23 ka), compared with 64 cores providing no Holocene (<10 ka) data, and 124 cores providing no data from Marine Isotope Stage (MIS) 5a or earlier (>71 ka). This is summarised in Table 1. The raw data and the δ^{18}O age model are included as Supplementary Materials. The raw data has undergone basic filtering; for example,

Table 1. Cores used in the data synthesis. Flags: R = mean data resolution poorer than 6 ka; r = mean data resolution poorer than 3 ka; H = at least one period of >20 ka with no obseravtions; h = at least one period of >10 ka with no observations; p = upwelling region or phytodetritus effect suspected; X = no processed data from record.

Core	Latitude	Longitude	Depth (m)	Ocean	Benthic species	Age (ka)	# of obs.	Sed. rate	Flag	Plank. species	Age (ka)	# of obs.	Sed. rate	Flag	Reference
PS2177−1	88.03	134.93	1388	Arct.						*N. pachyde*	2−76	38	0.6	h	Noer98
PS2185−3	87.52	144.38	1051	Arct.						*N. pachyde*	0−52	34	0.7		Noer98
PS2166−2	86.85	59.77	3636	Arct.						*N. pachyde*	2−73	39	0.6		Noer98
PS2138−1	81.54	30.88	862	Arct.	*C. teretis*	13−150	54	4.2	h						DELPHI
V27−64	73.52	20.00	479	Arct.						*N. pachyde*	10−14	8	75.0		DELPHI
V30−163	72.40	14.82	748	Arct.						*N. pachyde*	24−48	21	46.3		DELPHI
V28−14	64.78	−29.57	1855	Arct.						*N. pachyde*	0−>150	73	3.8		CDLS88
V29−202	61.00	−21.02	2658	Arct.	*C. wueller*	2−>150	184	5.2	p						OL95
V27−60	72.18	−8.58	2525	Arct.^{N}						*N. pachyde*	1−>150	73	4.2		DLB88
					C. wueller	1−133	41	4.2	rH						
PS1243−1	69.37	−6.55	2711	Arct.^{N}	*C. wueller*	1−30	57	2.8		*N. pachyde*	1−30	61	2.8		BESS01
V28−56	68.03	−6.12	2941	Arct.^{N}	*C. wueller*	108−125	9	2.9	p	*N. pachyde*	108−135	13	2.6		CLIMAP
					O. tener	108−125	9	2.9	p						
GIK23071	67.08	2.91	1308	Arct.^{N}							2−140	269	5.3		SV01
SO82_5−2	59.19	−30.90	1416	N Atl.	*C. wueller*	5−65	142	9.7	p	*N. pachyde*	5−47	72	9.4		Jung04
BOFS17K	58.00	−16.50	1150	N Atl.	*C. wueller*	2−49	35	2.8		*G. bulloid*	2−115	121	2.1		LMC94
ODP982	57.50	−15.88	1145	N Atl.	*Cib.* spp.	0−>150	62	2.5		*G. bulloid*	0−>150	66	2.5		VHSW99
NA87−22	55.50	−14.58	2161	N Atl.	*C. wueller*	0−25	49	25.5							DLAP92
ODP980	55.48	−14.72	2168	N Atl.	*C. wueller*	1−>150	138	14.0							OMC03
GIK17049−6	55.26	−26.73	3331	N Atl.	*C. wueller*	1−>150	123	4.1	h	*G. bulloid*	0−>150	166	4.1	h	JS03
GIK23419−8	54.96	−19.75	1491	N Atl.	*C. wueller*	3−110	147	7.0	h	*G. bulloid*	3−110	158	7.0		JS03b
										N. pachyde	0−41	95	4.0		
V27−20	54.00	−46.20	3510	N Atl.	*C. wueller*	91−148	22	2.3							CLIMAP
GIK23414−9	53.54	−20.29	2196	N Atl.	*C. wueller*	0−>150	178	3.2		Genus mix:	0−>150	182	3.2		JS03c
GIK23415−9	53.18	−19.14	2472	N Atl.	*C. wueller*	1−>150	183	4.0		*G. bulloid*	1−>150	144	4.0		JS03d
NEAP18K	52.77	−30.34	3275	N Atl.	*C. wueller*	55−126	184	5.6	p						CS99
SU90−39	52.57	−21.94	3955	N Atl.	*C. wueller*	10−140	152	6.9	p	*G. bulloid*	10−>150	146	8.0		Cort03
											14−>150	117	8.0	h	
GIK23418−8	52.55	−20.33	1491	N Atl.	*C. wueller*	0−>150	129	6.7	h	*G. bulloid*	0−>150	216	6.7		JS03e
GIK17045−3	52.42	−16.66	3663	N Atl.	*C. wueller*	8−>150	66	4.8	h						SWJD94
GEOB6728−1_ISO	52.15	−12.77	749	N Atl.	*C. kullenb*	2−48	80	9.6							DHRD05
GEOB6719−1	52.15	−12.77	758	N Atl.	*C. kullenb*	13−130	79	3.5							RDDH05
GIK23416−4	51.57	−20.00	3616	N Atl.	*C. wueller*	6−150	90	7.1	h	*G. bulloid*	6−150	144	7.1		JS04a
GIK23417−1	50.67	−19.43	3850	N Atl.	*C. wueller*	4−79	142	7.5		*N. pachyde*	6−79	111	7.6		JS03f
ODP851	46.22	−34.32	3760	N Atl.						*G. sacculi*	4−>150	25	1.9	rh	CR97
NO79−28	45.63	−22.75	3625	N Atl.	*U. peregri*	18−>150	105	5.0	H	*G. bulloid*	10−>150	67	5.0		Dupl96
V29−179	44.71	−24.53	3331	N Atl.	*Uvig.* spp.	20−150	74	4.1	h						CLIMAP
					C. wueller	2−130	34	4.0	rH						
					M. barlean	14−100	11	4.3	RH						
					H. elegans	2−16	8	3.6							
					Cib. spp.	2−9	4	2.2							
SU90−11	44.07	−40.02	3645	N Atl.	*C. wueller*	10−>150	67	3.6	h	*N. pachyde*	10−150	139	3.6		LVCP95
					U. excelle	12−149	108	3.6	h	*G. bulloid*	10−150	109	3.6		
CHN82−20	43.50	−29.87	3020	N Atl.	*C. wueller*	4−25	49	6.1		*G. bulloid*	4−23	43	6.1		DELPHI
MD952039	40.58	−10.35	3381	N Atl.	*C. wueller*	5−>150	173	10.8							LCO06
NO82−13	40.53	−10.43	3780	N Atl.	*C. wueller*	10−34	43	17.4		*G. bulloid*	10−65	77	14.5		Labe96
PO200_10_6−2	37.82	−9.50	1086	N Atl.	*Uvig.* spp.	2−41	46	14.4		*G. bulloid*	2−41	47	14.4		ABHR98
MD95−2042	37.80	−10.17	3146	N Atl.	*C. wueller*	2−150	258	20.1							SHV00
PO200/10_8−2.97	37.64	−9.93	2200	N Atl.	*C. wueller*	3−30	23	10.5		*G. bulloid*	2−30	31	10.7		ABHR98
KF09	37.11	−32.29	2655	N Atl.	*C. wueller*	2−31	12	16.0	h	*G. ruber*	2−31	45	16.0		Rich01
MD99−2339	35.89	−7.53	1177	N Atl.	benthic	2−47	184	40.4	p	*N. pachyde*	2−47	182	40.4		Voel06
					Uvig spp.	2−47	52	40.3	p						
V10−58	35.67	26.30	2283	N Atl.						*G. ruber*	1−36	42	15.1		CLIMAP
GIK11944−2	35.65	−8.06	1765	N Atl.	*C. wueller*	10−95	67	6.4							WS03
GIK15669−1	34.89	−7.82	2022	N Atl.	*C. wueller*	9−95	71	5.6							ZS03
GIK15672−1	34.86	−8.13	2460	N Atl.	*C. wueller*	4−57	42	4.3		*G. ruber*	4−55	40	4.3		SWJD94
EN120_GGC_1	33.67	−57.62	4450	N Atl.	*Cib* spp.	6−25	43	13.9							Keig04
KNR140−51GGC	32.78	−76.12	1790	N Atl.	*U. peregri*	5−18	41	32.3		*G. sacculi*	5−18	44	32.3		Keig04
KNR140−64GGC	32.74	−76.13	2101	N Atl.	*C. wueller*	14−24	18	13.8		*G. ruber*	2−29	52	13.9		Keig04
					U. peregri	1−23	12	13.9	h						
KNR140−67JPC	32.74	−76.13	2102	N Atl.	*N. umbonif*	10−30	32	10.8	p	*G. ruber*	10−29	22	11.2		Keig04
KNR140−43GGC	32.02	−76.07	2590	N Atl.	*U. peregr*	12−22	39	17.7		*G. ruber*	10−25	66	17.7		Keig04
KNR140−37JPC	31.41	−75.26	3000	N Atl.	*Cib* spp.	0−149	236	13.5							Keig04
					Uvig. spp.	8−61	164	22.8							
KNR140−30GGC	30.73	−74.47	3433	N Atl.	*U. peregri*	11−24	27	15.8		*G. ruber*	10−25	38	16.0		Keig04
GEOB4216−1	30.63	−12.40	2324	N Atl.	*C. wueller*	4−>150	127	4.5		*G. bulloid*	4−>150	130	4.5		FMHK02
GIK16004−1	29.98	−10.65	1512	N Atl.	*C. wueller*	4−139	60	3.3		*G. bulloid*	4−139	59	3.3		SWJD94
					Pyrgo murr	4−136	32	3.2	r	*G. ruber*	4−139	57	3.3		
										G. inflata	4−128	53	3.3		

Table 1. Continued.

Core	Latitude	Longitude	Depth (m)	Ocean	Benthic species	Age (ka)	# of obs.	Sed. rate	Flag	Plank. species	Age (ka)	# of obs.	Sed. rate	Flag	Reference
GIK15627−3	29.17	−12.09	1024	N Atl.	*C. wueller*	9−>150	49	3.2		*G. inflata*	7−>150	39	3.2	rh	SWJD94
KNR140−12JPC	29.07	−72.90	4250	N Atl.	*N. umbonif*	8−25	43	12.8		*G. ruber*	8−24	32	13.0		Keig04
GEOB4223−2	29.02	−12.47	775	N Atl.	*U. peregri*	1−98	150	7.8		*G. bulloid*	1−98	149	7.8		FMHK02
GEOB4240−2	28.89	−13.22	1358	N Atl.	*C. wueller*	5−137	59	4.9		*G. bulloid*	3−137	133	5.0		FMHK02
KNR140−22JPC	28.02	−74.41	4712	N Atl.	*N. umbonif*	12−21	20	17.3	p	*G. ruber*	9−21	43	17.3		Keig04
GIK15637−1	27.00	−18.99	3849	N Atl.	*C. wueller*	10−>150	41	2.0	rh						ZS03b
OCE205−149GGC	26.26	−77.67	423	N Atl.	*C. kullenb*	8−44	26	6.8							SC95
OCE205−7JPC	26.14	−77.23	1320	N Atl.	*C. kullenb*	0−69	26	2.6							SC95
					H. elegans	0−137	35	2.0	r						
OCE205−103GCC	26.07	−78.07	965	N Atl.	*C. cicatri*	3−62	42	4.6	p						SC95
					C. kullenb	3−61	100	4.6	p						
OCE205−108GGC	25.98	−78.18	743	N Atl.	*P. arimine*	6−22	28	15.2							SC95
					C. pachyde	0−23	33	10.7							
OCE106GGC	25.98	−78.18	423	N Atl.	*C. cicatri*	6−25	23	7.5							SC95
					C. corpule	6−25	21	7.5							
					C. pachyde	6−25	20	7.5							
					H. elegans	6−25	23	7.5							
					P. arimine	6−25	23	7.5							
					P. foveola	6−22	10	7.5							
					P. roberts	6−25	22	7.5							
GIK12392−1	25.17	−16.84	2575	N Atl.	*C. wueller*	3−141	113	6.9							ZWS86
BOFS28K	24.64	−22.81	4900	N Atl.	*C. wueller*	4−30	20	1.9	p						BES95
BOFS26K	24.48	−19.89	3680	N Atl.	*C. wueller*	4−26	20	1.9							BES95
GIK16017−2	21.25	−17.80	812	N Atl.	*C. wueller*	6−37	57	13.2		*G. ruber*	6−38	55	13.1		SWJD94
GIK16030−1	21.23	−18.05	1516	N Atl.	*C. wueller*	4−109	65	9.6		*G. bulloid*	4−38	43	8.6		SWJD94
					U. peregri	4−35	28	8.4		*G. ruber*	4−38	43	8.6		
										G. inflata	4−38	43	8.6		
GIK12328−5	21.14	−18.57	2798	N Atl.	*C. wueller*	0−47	67	11.8		*G. ruber*	0−49	65	11.9		SWJD94
ODP658C	20.75	−18.58	2273	N Atl.	*C. wueller*	0−50	120	12.6		*G. bulloid*	0−50	113	12.6		ZBSS95
										G. inflata	0−50	118	12.6		
										G. ruber	0−50	120	12.6		
										G. ruber	0−49	113	12.6		
BOFS29K	20.53	−21.11	4000	N Atl.	*C. wueller*	0−32	26	2.8							BES95
V30−49	18.43	−21.10	3093	N Atl.						*C. wueller*	2−28	30	4.3		CDLS88
GIK13289−2	18.07	−18.01	2485	N Atl.	*C. wueller*	3−31	30	6.5							SWJD94
					U. peregri	3−31	26	6.5							
GIK12337−4AND 5	15.95	−18.13	3094	N Atl.	*C. wueller*	10−17	28	19.5		*G. ruber*	10−17	28	19.5		SWJD94
GIK16402−1	14.42	−20.57	4203	N Atl.	*C. wueller*	6−>150	33	2.1	rh	*G. sacculi*	5−22	12	3.9		SWJD94
V22−197	14.17	−18.58	3167	N Atl.	*Uvig.* spp.	1−>150	87	5.1							CDLS88
GIK13239−1	13.88	−18.31	3156	N Atl.	*C. wueller*	8−40	48	13.7							SWJD94
					U. hollick	8−40	45	13.7							
V22−196	13.83	−18.96	3728	N Atl.	*C. wueller*	3−19	13	5.1							CLIMAP
M35003−4	12.09	−61.24	1299	N Atl.	Cib. spp.	1−57	96	16.6	p						Huel99
					Uvig. spp.	24−58	53	16.6	p						
V22−108	9.92	−20.98	4956	N Atl.						*G. bulloid*	1−133	29	4.1	rH	CLIMAP
GIK16408−2	9.01	−21.46	4239	N Atl.	*C. wueller*	2−18	10	2.3		*G. ruber*	0−18	12	2.3		SWJD94
GIK16408−5	9.01	−21.50	4336	N Atl.	*C. wueller*	2−27	11	2.2							SWJD94
GIK16459−1	7.28	−26.19	4835	N Atl.	*C. wueller*	8−36	30	3.1		*G. ruber*	8−21	18	3.1		SWJD94
GEOB4403−2	6.13	−43.44	4503	N Atl.	*C. wueller*	1−>150	136	3.4	H						BM03
ODP929	5.98	−43.74	4356	N Atl.	*C. wueller*	10−>150	52	5.8							BCW97
					C. cicatri	24−>150	11	5.6	RH						
GIK13519−1	5.67	−19.85	2862	N Atl.	*C. wueller*	1−>150	79	1.3							SWJD94
					U. hollick	13−144	34	1.4	rh						
ODP927	5.46	−44.48	3315	N Atl.	*C. wueller*	10−>150	56	5.3	p						CO05
					Cib. spp.	26−>150	11	5.3	RHp						
EW9209−1JPC	5.00	−43.00	4056	N Atl.	*C. wueller*	1−150	229	3.8	p						CO97
KN11002−0055	4.95	−42.89	4556	N Atl.	*C. wueller*	5−63	40	2.2							CDLS88
KN11002−0050PG	4.87	−43.20	3995	N Atl.	*C. wueller*	12−47	40	3.8	p						CDLS88
GIK16856−2	4.80	3.40	2861	N Atl.		8−74	43	4.7							SWJD94
KN11002−0058	4.79	−43.04	4341	N Atl.	*C. wueller*	4−43	38	3.3							CDLS88
KN11002−0066PG	4.56	−43.38	3547	N Atl.	*C. wueller*	2−39	40	3.6							CDLS88
GEOB1520−1	4.49	−41.93	3911	N Atl.	*C. wueller*	6−>150	80	1.8							BM03
KN11002−0071PG	4.36	−43.70	3164	N Atl.	*C. wueller*	1−42	44	3.5							CDLS88
KN11002−0075	4.34	−43.41	3063	N Atl.	*C. wueller*	4−72	40	1.9							CDLS88
ODP925	4.20	−43.49	3041	N Atl.	*C. wueller*	10−>150	39	4.3	rH						BCW97
					C. bradyii	18−>150	18	4.2	RH						
GEOB1523−2	3.83	−41.62	3291	N Atl.	*C. wueller*	2−>150	61	2.0							Muli98
GIK13521−1	3.02	−22.03	4504	N Atl.	*C. wueller*	7−>150	25	2.4	rH	*G. sacculi*	7−>150	27	2.7	rh	SWJD94
GEOB1505−2	2.27	−33.02	3706	N Atl.											ZBDH99
					C. wueller	10−>150	63	2.0							
GEOB1101−5	1.66	−10.98	4588	N Atl.	*C. wueller*	8−>150	36	1.4	r						BW96
GIK16771−2	0.82	−15.51	2764	N Atl.	*C. wueller*	4−87	11	2.1	RH	*G. sacculi*	4−>150	30	2.0	rh	SWJD94
										G. ruber	4−>150	30	2.0	rh	

Table 1. Continued.

Core	Latitude	Longitude	Depth (m)	Ocean	Benthic species	Age (ka)	# of obs.	Sed. rate	Flag	Plank. species	Age (ka)	# of obs.	Sed. rate	Flag	Reference
12PC51	0.01	−23.00	3870	N Atl.						*G. sacculi*	9−47	44	2.5		SK94
GEOB2215−10	0.01	−23.50	3711	N Atl.	*C. wueller*	8−30	24	5.5							BM03
GIK16773−1	−0.97	−9.44	4662	S Atl.	*C. wueller*	0−17	29	3.3		*G. ruber*	0−17	29	3.3		SWJD94
GIK16772−1	−1.34	−11.97	3911	S Atl.	*C. wueller*	14−>150	56	4.6		*G. sacculi*	14−>150	58	4.6		SWJD94
GIK12329−6	−1.35	−19.93	3912	S Atl.	*C. wueller*	4−43	23	3.1							SWJD94
					Pyrgo spp.	70−>150	25	2.8	r						
GEOB1105−4	−1.67	−12.43	3225	S Atl.	*C. wueller*	8−>150	123	4.1							BW96
GIK16867−2	−2.20	5.10	3891	S Atl.	*C. wueller*	8−137	48	2.7		*G. ruber*	8−137	50	2.7		SWJD94
RC13−205	−2.29	5.18	3731	S Atl.						*G. ruber*	3−22	11	6.3		CLIMAP
GEOB1041−3	−3.48	−7.60	4033	S Atl.							5−>150	56	2.1		BW96
GEOB1118−2	−3.56	−16.43	4675	S Atl.	*C. wueller*	6−>150	67	2.1	p						BW96
GEOB1115−3	−3.56	−12.56	2945	S Atl.	*C. wueller*	1−>150	102	3.2	p						BW96
GEOB1501−4	−3.68	−32.01	4257	S Atl.	*C. wueller*	10−28	14	3.6							DHMP97
GEOB1112−4	−5.78	−10.75	3125	S Atl.	*C. wueller*	3−>150	74	2.6	p						BW96
V12−70	−6.48	11.43	450	S Atl.	*P. arimine*	12−43	28	6.4		*G. sacculi*	12−43	28	6.4		LCO06
GEOB1903−3	−8.68	−11.85	3161	S Atl.	*C. wueller*	8−30	15	3.2	p						DHMP97
V22−38	−9.55	−34.25	3797	S Atl.	*C. wueller*	78−135	16	1.4	rhp	*G. sacculi*	78−135	35	1.4		CLIMAP
V22−174	−10.07	−12.82	2630	S Atl.	*Uvig.* spp.	0−130	41	2.4	r						MRKM89
ODP1079	−11.93	13.31	755	S Atl.	C. pachyde	0−20	34	42.5							LCO06
					Planulina	0−20	29	26.4							
GEOB1417−1	−15.54	−12.71	2845	S Atl.	*C. wueller*	10−23	14	5.0							BM03
V29−135	−19.70	8.88	2675	S Atl.	*C. wueller*	4−>150	57	3.4	hp						SWJD94
GEOB1028−5	−20.10	9.19	2209	S Atl.	*C. wueller*	3−>150	90	2.6							WBBD96
V19−258	−20.40	11.62	965	S Atl.	C. pachyde	8−29	20	11.3		*G. bulloid*	8−30	40	11.1		LCO06
GEOB5115−2	−21.14	−14.04	3291	S Atl.	*C. wueller*	4−23	22	1.1							BM03
GEOB1035−3	−21.60	5.03	4450	S Atl.	*C. wueller*	6−>150	37	1.3	rp						BW96
GEOB3202−1	−21.62	−39.98	1090	S Atl.	*U. peregri*	10−62	98	9.4		*G. sacculi*	10−62	98	9.4		APW99
										G. ruber	10−62	99	9.4		
GEOB1034−3	−21.73	5.42	3772	S Atl.	*C. wueller*	7−>150	33	0.8	r						BW96
RC13−228	−22.33	11.20	3204	S Atl.	*C. wueller*	1−136	54	5.0	Hp						CDLS88
					Uvig. spp.	116−150	10	3.4	rhp						
GEOB1032−3	−22.91	6.04	2505	S Atl.	*C. wueller*	6−>150	43	1.4	rp						BW96
GEOB1710−3	−23.43	11.70	2987	S Atl.	*C. wueller*	2−>150	151	5.4							SM97
RC8−39	−24.07	−15.12	3977	S Atl.						*G. bulloid*	10−136	52	7.0	H	CLIMAP
GEOB1211−3	−24.47	7.54	4089	S Atl.	*C. wueller*	6−>150	37	0.7	rhp						BW96
V19−248	−24.57	4.83	3321	S Atl.						*G. ruber*	5−32	8	1.8	r	CLIMAP
GEOB1214−1	−24.69	7.24	3210	S Atl.	*C. wueller*	3−>150	35	1.2	r						SM97
RC13−229	−25.49	11.31	4191	S Atl.	*Uvig.* spp.	1−>150	37	2.2	rhp						OFGS90
ODP1084B	−25.51	13.03	1992	S Atl.	*C. wueller*	7−19	18	26.5							LCO06
GEOB2109−1	−27.91	−45.88	2504	S Atl.	*C. wueller*	6−>150	106	2.7							DHMP97
V20−220	−28.60	−29.02	3601	S Atl.	Orid. spp.	15−27	7	20.5							DELPHI
										G. pseudoa	21−27	8	20.5		
GEOB1721−6	−29.17	13.08	3044	S Atl.	*C. wueller*	0−>150	78	2.6							BM03
GEOB1722−3	−29.49	11.75	3973	S Atl.	*C. wueller*	1−>150	50	1.3							MSMS02
GEOB3801−6	−29.51	−8.31	4546	S Atl.	*C. wueller*	8−>150	33	1.3	r						BM03
V19−240	−30.58	13.28	3103	S Atl.	*C. wueller*	2−35	13	3.1							LCO06
GEOB2004−2	−30.87	14.34	2569	S Atl.	*C. wueller*	4−30	33	6.2							BM03
ODP1087	−31.46	15.31	1372	S Atl.	*C. wueller*	0->150	69	2.5							PSUG01
GEOB1312−2	−31.66	−29.66	3436	S Atl.	*C. wueller*	9->150	23	0.9	RpX	*G. ruber*	9−>150	23	0.9	R	HP99
V19−236	−33.88	17.63	280	S Atl.	C. pachyde	9−26	34	20.0		*G. bulloid*	9−26	34	20.0		LCO06
					P. arimine	8−26	20	20.0							
GEOB3603−2	−35.13	17.54	2840	S Atl.	*C. wueller*	12−>150	87	3.2							BM03
RC11−86	−35.78	18.45	2829	S Atl.						*G. sacculi*	7−27	14	3.2		CLIMAP
					Var. benth	7−27	14	3.2							
GEOB2019−1	−36.06	−8.78	3825	S Atl.	*C. wueller*	6−30	14	2.9	p						BM03
MD96−2080	−36.27	19.48	2488	S Atl.	*C. wueller*	1−>150	35	1.9	rp	*G. inflata*	1−>150	35	1.9	r	RRLG02
RC12−294	−37.27	−10.12	3308	S Atl.	*Uvig.* spp.	13−>150	73	2.9							IMM97
					C. wueller	16−>150	19	2.8	RH						
RC12−267	−38.68	−25.78	4144	S Atl.	*Uvig.* spp.	9−20	7	9.2							CLIMAP
ODP1089	−40.94	9.89	4621	S Atl.^{S}	Cib. spp.	3−>150	382	15.5	p	*G. bulloid*	1−>150	400	15.4		HVCN03
ODP1088	−41.14	13.56	2082	S Atl.^{S}	Cib. spp.	3−>150	29	1.3	rhp						HVCN03
PS2495−3	−41.27	−14.49	3134	S Atl.^{S}	Cib. spp.	10−>150	43	3.0	r						MGHK94
ODP1090	−42.91	8.90	3702	S Atl.^{S}	Cib. spp.	6−145	79	3.5	h						HVCN03
					C. wueller	6−>150	79	2.0	h	*G. bulloid*	5−>150	168	2.0		
					C. kullenb	7−>150	60	3.0	H						
										N. pachyde	7−>150	151	3.0		
RC15−94	−42.98	−20.86	3762	S Atl.^{S}						*G. inflata*	9−29	25	12.1		CLIMAP
PS2082−1	−43.22	11.74	4610	S Atl.^{S}	Cib. spp.	10−>150	68	4.4	hp	*N. pachyde*	10−>150	71	4.4		MGHK94
										G. bulloid	10−>150	71	4.4		
PS2498−1	−44.15	−14.23	3783	S Atl.^{S}	Cib. spp.	6−135	96	9.0							MRK01
ODP704A	−46.88	7.42	2543	S Atl.^{S}	Cib. spp.	9−>150	18	2.8	RHp	*N. pachyde*	9−>150	26	2.8	rh	HVCN03
					Gyroidina	9−>150	19	2.8	Rhp						

Table 1. Continued.

Core	Latitude	Longitude	Depth (m)	Ocean	Benthic species	Age (ka)	# of obs.	Sed. rate	Flag	Plank. species	Age (ka)	# of obs.	Sed. rate	Flag	Reference
RC13−269	−52.63	0.12	2591	S Atl.^{S}	*Uvig.* spp.	9−90	40	6.1	p						CLIMAP
PS1506	−68.73	−5.85	2426	S Atl.^{S}	E. Exigua	0−>150	67	0.8	h	*N. pachyde*	0−>150	82	0.8		RERH09
M5−3A−422	24.39	58.04	2732	Ind.	*C. wueller*	1−25	91	9.2		*G. ruber*	0−24	84	9.3		SGD00
SO90−93K	23.59	64.22	1802	Ind.						*G. ruber*	36−68	50	3.3		SVE98
										G. ruber	68−81	44	8.1		
ORGON4−KS8	23.47	59.19	2900	Ind.	*C. wueller*	10−39	61	19.9		*G. ruber*	10−36	58	21.1		SGD00
V34−88	16.54	59.76	2171	Ind.	*Uvig.* spp.	100−144	24	3.5	p	*G. sacculi*	100−144	32	3.5		CLIMAP
SK17	15.25	72.73	840	Ind.						*G. ruber*	4−25	58	2213.0		Anandpc
										G. bulloid	4−25	57	2213.0		
GEOB3004−1	14.61	52.92	1803	Ind.	*C. wueller*	0−>150	163	5.3							SM06
SO42−74KL	14.33	57.35	3212	Ind.											SSEL93
					C. wueller	1−47	107	6.7	p	*G. ruber*	1−47	123	6.7		
IOE105KK	11.27	53.54	3535	Ind.						*G. ruber*	2−30	20	6.8		Siro02
905	10.46	51.56	1580	Ind.	*C. wueller*	0−26	27	23.3		*G. ruber*	0−26	31	23.3		JKGP09
										G. bulloid	0−26	31	23.3		
RC12−339	9.13	90.03	3010	Ind.	*C. wueller*	99−138	22	1.8		*G. sacculi*	99−138	36	1.8		CLIMAP
V19−178	8.12	73.27	2188	Ind.						*G. ruber*	7−25	8	3.6		PHWB80
V19−188	6.87	60.67	3356	Ind.						*G. ruber*	3−30	16	3.2		CLIMAP
										G. sacculi	2−30	17	3.2		
V29−29	5.12	77.58	2673	Ind.						*G. sacculi*	83−147	37	2.8		CLIMAP
MD900963	5.05	73.90	2446	Ind.							10−>150	86	4.4		BBVL94
V29−31	3.80	78.65	3793	Ind.						G. menardi	5−15	11	10.0		DELPHI
RC14−37	1.47	90.17	2226	Ind.						*G. ruber*	10−21	10	6.4		CLIMAP
MD01−2378	−13.08	121.79	1783	Ind.	*C. wueller*	0−150	156	10.5	p						KHK06
RC17−98	−13.22	65.62	3409	Ind.						*G. sacculi*	108−>150	17	2.3		CLIMAP
V28−345	−17.67	117.95	1904	Ind.	*Uvig.* spp.	102−150	8	2.1	RHp	*G. sacculi*	100−150	26	2.1		CLIMAP
						125−150	10	2.4	p						
						117−146	9	2.2	rp						
182−1132B	−33.32	127.60	219	Ind.	*U. peregri*	18−>150	52	36.3							HKJ02
E49−21	−42.18	94.90	3328	Ind.^{S}						planktonic	2−>150	28	1.9	rh	CLIMAP
RC08−39	−42.88	42.35	4330	Ind.^{S}						*G. bulloid*	114−137	30	6.4		CLIMAP
RC11−120	−43.31	79.52	3193	Ind.^{S}	*Uvig.* spp.	3−115	63	3.5	p						MPHI87
					Globocas.	3−115	37	3.5	rhp						
					C. wueller	3−130	34	3.4	rHp						
										G. bulloid	3−>150	98	3.2		
ELT45029−PC	−44.88	106.52	3867	Ind.^{S}						*G. bulloid*	10−>150	33	3.1	r	CLIMAP
MD88−770	−46.02	96.46	3290	Ind.^{S}	*C. wueller*	7−17	9	9.1	p						Labe98
ELT49018−PC	−46.05	90.16	3282	Ind.^{S}						*G. bulloid*	12−140	56	4.3		CLIMAP
E49−23	−47.12	95.10	3206	Ind.^{S}						planktonic	4−118	57	5.1		HP94
ELT49023−PC	−47.13	95.08	3285	Ind.^{S}							12−116	57	5.5		HP94
ELT49017−PC	−48.28	90.25	3546	Ind.^{S}						*G. bulloid*	18−>150	46	2.2		HP94
V36−06	19.43	115.90	2387	N Pac.^{SC}						*G. sacculi*	0−109	112	10.9		DELPHI
GGC−6	12.15	118.06	2975	N Pac.^{SC}						*G. sacculi*	8−50	30	3.5		TQCP92
GGC−12	11.93	118.21	2495	N Pac.^{SC}							6−36	28	4.6		TQCP92
GGC−11	11.89	118.33	2165	N Pac.^{SC}						*G. sacculi*	6−40	29	4.1		TQCP92
GGC−10	11.72	118.51	1605	N Pac.^{SC}						*G. sacculi*	4−37	29	4.4		TQCP92
GGC−13	10.60	118.29	990	N Pac.^{SC}						*G. sacculi*	1−33	30	4.5		TQCP92
ODP1143	9.36	113.29	2772	N Pac.^{SC}	*C. wueller*	5−147	60	6.7	h						TWCL02
V35−05	7.20	112.08	1953	N Pac.^{SC}	*C. wueller*	2−19	12	20.5							OF87
RC23−50B	1.03	104.41	3473	N Pac.^{SC}	*Uvig.* spp.	8−15	21	5.0	p						DELPHI
V32−161	48.28	149.07	1600	N Pac.	*Uvig.* spp.	0−48	24	5.0	h						MHS91
Y2711−1	43.26	−126.38	2913	N Pac.	*Uvig.* spp.	112−142	37	5.2							CLIMAP
J−11	40.13	−134.00	1150	N Pac.						*N. pachyde*	6−28	61	6.6		GS00
V32−128	36.47	177.17	3623	N Pac.	*C. wueller*	0−>150	34	2.7	rh						CLIMAP
					Uvig. spp.	2−>150	5	3.6	RHX						
V32−126	35.32	177.92	3870	N Pac.	Var. benth	3−133	18	4.6	RH						CLIMAP
RC10−175	34.58	159.17	4014	N Pac.	Var. benth	8−20	6	3.8							DELPHI
V28−304	28.53	134.13	2942	N Pac.	*C. wueller*	0−>150	46	4.5	rh						CDLS88
					Uvig. spp.	0−>150	62	4.5	h						
					Cib. spp.	8−37	15	6.6							
V28−294	28.43	139.97	2308	N Pac.	*Uvig.* spp.	31−80	26	4.7							CLIMAP
RC12−36	14.74	−97.67	3354	N Pac.	*Uvig.* spp.	12−19	6	2.7	p						DELPHI
V28−240	5.22	158.07	1767	N Pac.						G. fistulo	24−46	49	21.8		DELPHI
V28−179	4.62	−139.60	4502	N Pac.	Globocas.	18−107	107	2.4							DELPHI
RC17−176	3.75	158.77	3156	N Pac.						*G. sacculi*	17−26	18	0.4		DELPHI
V17−42	3.53	−81.18	1814	N Pac.						*G. ruber*	12−21	5	5.8		DELPHI
										G. sacculi	9−21	7	5.8		
V19−25	2.47	−81.70	2404	N Pac.						G. dutertr	6−37	40	6.3		DELPHI
RC13−138	1.81	−94.14	2655	N Pac.						*G. sacculi*	1−>150	201	4.8		DELPHI
ODP805C	1.23	160.53	3188	N Pac.	*C. wueller*	16−>150	18	1.3	Rhp						LPS00
V28−238	1.02	160.48	3120	N Pac.						*G. sacculi*	3−>150	48	1.8	r	CLIMAP
V21−29	0.95	−89.35	712	N Pac.	*Uvig.* spp.	3−23	9	8.0	p						DELPHI
V24−109	0.43	158.80	2367	N Pac.	*C. wueller*	0−80	103	3.4	p						SLMH92

Table 1. Continued.

Core	Latitude	Longitude	Depth (m)	Ocean	Benthic species	Age (ka)	# of obs.	Sed. rate	Flag	Plank. species	Age (ka)	# of obs.	Sed. rate	Flag	Reference
										G. sacculi	1−>150	93	1.4		
ODP806B	0.32	159.36	2520	N Pac.	*C. wueller*	3−>150	31	2.6	rhp	*G. sacculi*	3−>150	31	2.9	rh	LPS00
RC13−110	0.00	−96.02	3231	N Pac.	*C. wueller*	5−>150	63	2.0	h						MPZR91
V19−27	−0.47	−82.08	1373	S Pac.											MPZR91
					C. wueller	3−150	71	2.5							
RC10−65	−0.69	−108.62	3588	S Pac.						*G. sacculi*	11−20	21	6.7		DELPHI
										Pulleniati	11−20	24	7.8		
										G. tumida	11−45	47	11.7		
RC10−97	−0.92	−134.31	4305	S Pac.	Var. benth	5−25	6	2.4	r						DELPHI
V19−28	−2.37	−84.65	2720	S Pac.	*Uvig.* spp.	0−>150	67	4.4	p						DELPHI
RC10−140	−2.65	156.98	1679	S Pac.						*G. sacculi*	14−30	10	5.6		DELPHI
ODP846	−3.08	−90.83	3296	S Pac.	*C. wueller*	8−>150	56	3.7							SHP95
					U. peregri	99−>150	14	3.7	r						
V19−30	−3.57	−83.23	3157	S Pac.	benthic	0−>150	297	5.3	p						CDLS88
V28−235	−5.45	160.48	1746	S Pac.						*G. sacculi*	2−>150	26	1.3	r	CLIMAP
V24−184	−12.87	146.22	2992	S Pac.						*G. sacculi*	5−>150	15	1.3	Rh	APB89
V24−170	−13.52	146.90	2243	S Pac.						*G. sacculi*	2−>150	21	1.4	R	APB89
RC10−131	−14.53	157.97	2933	S Pac.						*G. sacculi*	3−65	25	3.9		APB89
MW91−15	−14.53	157.98	3296	S Pac.						*G. sacculi*	4−34	32	2.1		PT97
V24−166	−16.52	150.78	781	S Pac.						*G. sacculi*	2−10	13	30.0		APB89
V24−161	−18.20	151.47	1670	S Pac.						*G. sacculi*	25−89	19	2.8	r	APB89
MD06−3018	−23.00	166.15	2470	S Pac.	*C. wueller*	4−>150	35	1.6	r						REKC09
RC12−113	−24.88	163.53	2454	S Pac.						*G. sacculi*	8−76	24	3.5		APB89
RC12−109	−25.88	157.88	2930	S Pac.						*G. sacculi*	5−>150	22	1.5	R	APB89
RC15−52	−29.24	−85.98	3780	S Pac.	*Uvig.* spp.	10−30	11	2.2	p						CLIMAP
CHAT10K−1	−40.03	180.00	3003	S Pac.^{S}	*Uvig.* spp.	0−31	83	10.6	p	*G. bulloid*	0−31	83	10.6		MCH08
										G. inflata	0−31	83	10.6		
MD97−2121	−40.38	177.99	3014	S Pac.^{S}	*Uvig.* spp.	0−140	134	24.8	p	*G. inflata*	0−140	156	24.8		CMGN08
					Cib. spp.	1−132	57	24.9	Hp						
P69	−40.38	178.00	2195	S Pac.^{S}	benthic	6−26	33	30.2	p						WCN98
S794	−40.40	178.00	2195	S Pac.^{S}						*G. bulloid*	0−126	48	0.0		WCN98
CHAT5K	−40.78	−171.55	4240	S Pac.^{S}	*Uvig.* spp.	6−>150	32	1.0	rhp	*G. bulloid*	11−>150	21	1.0	RH	MCH08
CHAT1K	−41.58	−171.52	3556	S Pac.^{S}	*Uvig.* spp.	2−>150	84	2.1							WCN98
R657	−42.38	−178.49	3284	S Pac.^{S}	*Uvig.* spp.	6−>150	26	1.9	r	*G. bulloid*	3−>150	28	1.9	r	WCN98
CHAT3K	−42.66	−167.50	4802	S Pac.^{S}	*Uvig.* spp.	8−>150	125	1.9	h	*G. bulloid*	8−>150	129	1.9		MCH08
										G. inflata	8−>150	129	1.9		
U938	−45.08	179.50	2700	S Pac.^{S}	*Uvig.* spp.	5−95	39	0.0	hp	*G. bulloid*	6−95	42	0.0		WCN98
RC15−62	−45.29	−77.21	2809	S Pac.^{S}	*Uvig.* spp.	10−15	5	7.2	p						DELPHI
MD97−2120	−45.53	174.93	1210	S Pac.^{S}	Genus mix:	2−>150	480	10.7							PZES03
DSDP594	−45.59	175.08	1204	S Pac.^{S}	*Uvig.* spp.	4−>150	158	12.9	p	*G. bulloid*	4−>150	179	12.9		WCN98
Q200	−45.99	172.03	1370	S Pac.^{S}	benthic	5−120	22	2.4	rhp	planktonic	5−120	32	2.4	r	WCN98
RC12−225	−53.66	−123.13	2964	S Pac.^{S}						*G. bulloid*	8−51	42	8.1		RE99

Abbreviations are as follows. In header rows: Plank = planktonic; # of obs. = number of observations in core; Sed. rate = mean sedimentation rate (cm/ka) over period of data; all latitudes and longitudes in decimal degrees. In Ocean column: Arct. = Arctic Ocean; Arct^{N} = Nordic seas; ^{C} = Caribbean Sea; ^{S} = Southern Ocean (defined as >40 °S); ^{SC} = South China Sea. In Flag columns; R = mean data resolution poorer than 6 ka; r = mean data resolution poorer than 3 ka; H = at least one period of >20 ka with no obseravtions; h = at least one period of >10 ka with no observations; p = upwelling region or phytodetritus effect suspected; X = no processed data from record. Relevant references are as follows: ABHR98 = Abrantes et al. (1998); APB89 = Anderson et al. (1989); APW99 = Arz et al. (1999); Anandpc = P. Anand (personal communication); BBVL94 = Bassinot et al. (1994); BCW97 = Bickert et al. (1997); BES95 = Beveridge et al. (1995); BESS01 = Bauch et al. (2001); BM03 = Bickert and Mackensen (2003); BW96 = Bickert and Wefer (1996); CDLS88 = Curry et al. (1988); CLIMAP = Ruddiman and CLIMAP Project Members (1997); CMGN08 = Carter et al. (2008); CO05 = Curry and Oppo (2005); CO97 = Curry and Oppo (1997); CR97 = Cannariato and Ravelo (1997); CS99 = Chapman and Shackleton (1999); Cort03 = Cortijo (2003); DELPHI = Delphiproject, http://www.esc.cam.ac.uk/research/research-groups/delphi; DHMP97 = Dürkop et al. (1997); DHRD05 = Dorschel et al. (2005); DLAP92 = Duplessy et al. (1992); DLB88 = Duplessy et al. (1988a); Dupl96 = Duplessy (1996); FMHK02 = Freudenthal et al. (2002); GS00 = Gorbarenko and Southon (2000); HKJ02 = Holbourn et al. (2002); HP94 = Howard and Prell (1994); HP99 = Hale and Pflaumann (1999); HVCN03=Hodell et al. (2003); Huel99 = Hüls (1999); IMM97 = Imbrie et al. (1997); JKGP09 = Jung et al. (2009); JS03 = Jung and Sarnthein (2004a); JS03b=Jung and Sarnthein (2003a); JS03c=Jung and Sarnthein (2003b); JS03d = Jung and Sarnthein (2003c); JS03e = Jung and Sarnthein (2003d); JS03f = Jung and Sarnthein (2003e); JS04a = Jung and Sarnthein (2004b); Jung04 = Jung (2004); KHK06 = Kawamura et al. (2006); Keig04 = Keigwin (2004); LCO06 = Lynch-Stieglitz et al. (2006); LMC94 = Lowry et al. (1994); LPS00 = Lea et al. (2000); LVCP95 = Labeyrie et al. (1995); Labe96 = Labeyrie (1996); Labe98 = Labeyrie (1998); MCH08 = McCave et al. (2008), cores excluded from Supplementary Materials; MGHK94 = Mackensen et al. (1994); MHS91 = Morley et al. (1991); MPHI87 = Martinson et al. (1987); MPZR91 = Mix et al. (1991); MRK01 = Mackensen et al. (2001); MRKM89 = McIntyre et al. (1989); WS03 = Weinelt and Sarnthein (2003); MSMS02 = Mollenhauer et al. (2002); Muli98 = Mulitza (1998); Noer98 = Nrgaard-Pedersen et al. (1998); OF87 = Oppo and Fairbanks (1987); OFGS90 = Oppo et al. (1990); OL95 = Oppo and Lehmann (1995); OMC03 = Oppo et al. (2003); PHWB80 = Prell et al. (1980); PSUG01 = Pierre et al. (2001); PT97 = Patrick and Thunell (1997); PZES03 = Pahnke et al. (2003); RDDH05 = Rüggeberg et al. (2005); RE99 = Rickaby and Elderfield (1999); REKC09 = Russon et al. (2009); RERH09 = Rickaby et al. (2009); RRLG02 = Rau et al. (2002); Rich01 = Richter (2001); SC95 = Slowey and Curry (1995); SGD00 = Sirocko et al. (2000); SHP95 = Shackleton et al. (1995); SHV00 = Shackleton et al. (2000); SK94 = Sikes and Keigwin (1994); SLMH92 = Shackleton et al. (1992); SM06 = Schmiedl and Mackensen (2006); SM97 = Schmiedl and Mackensen (1997); SSEL93 = Sirocko et al. (1993); SV01 = Sarnthein and Voelker (2001); SVE98 = Schulz et al. (1998); SWJD94 = Sarnthein et al. (1994); Siro02 = Sirocko (2002); TQCP92 = Thunell et al. (1992); TWCL02 = Tian et al. (2002); VHSW99 = Venz et al. (1999); Voel06 = Voelker (2006); WBBD96 = Wefer et al. (1996a); WCN98 = Weaver et al. (1998); ZBDH99 = Zabel et al. (1999); ZBSS95 = Zhao et al. (1995); ZS03 = Zahn-Knoll and Sarnthein (2003a); ZS03b = Zahn-Knoll and Sarnthein (2003b); ZWS86 = Zahn et al. (1986). Where species names are abbreviated, full names are given in Table 2, except: C. cicatri = Cibicidoides cicatricosus; C. corpule = Cibicides corpulentus; C. kullenb = Cibicidoides kullenbergi; C. pachyde = Cibicidoides pachyderma; C. teretis = Cassidulina teretis; E. exigua = Epistominella exigua; Globocas = Globocassidulina species; Gyroidina = Gyroidina species; M. barlean = Melonis barleanum; N. umbonif = Nuttallides umbonifera; O. tener = Oridorsalis tener; Orid. spp. = Oridorsalis species; P. arimine = Planulina ariminensis; P. foveola = Planulina foveolata; P. roberts = Planulina robertsoniensis; Pyrgo murr = Pyrgo murrhina; U. excelle = Uvigerina excellens; U. hollick = Uvigerina hollicki; U. peregri = Uvigerina peregrina; Var. benth = record includes observations from more than one benthic genus, distinguished in raw date file; benthic = mixed benthics; G. dutertr = Globoquadrina dutertri; G. inflata = Globorotalia inflata; G. menardi = Globorotalia menardii; G. pseudoa = Globigerina pseudoampliapertura; Pulleniati = Pulleniatina species; Genus mix: = data from more than one genus, defined in raw date file; planktonic = mixed planktonics.

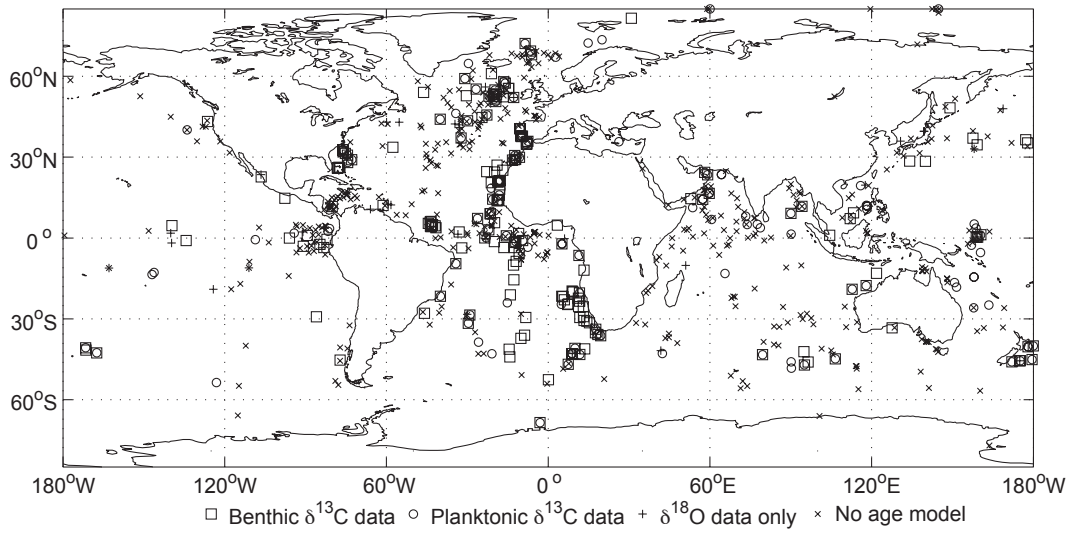

Fig. 2. Core locations of records included in the pre-processed data synthesis, or excluded because no δ^{18}O-derived age model could be constructed. For most excluded records, there were too few data (often true of cores sampled only at the LGM and/or Holocene), or the sampling resolution was targeted at longer timescales than a glacial cycle. The inclusion of records in the pre-processed synthesis was not explicitly constrained by data quality.

where records consisted principally of data from a single species, but with additional observations from other species, these additional observations were removed. We caution that this is not a primary source of raw data, which should instead be obtained from PANGAEA, NGDC, or Delphi. The fully processed data, after applying the methods described in Sect. 3, are included as Supplementary Materials.

2.2 Age modelling

For this study it was necessary to construct consistent age models for all cores. Since the accuracy required of these age models is rather low (a good representation of precessional and longer timescale variability is sufficient), we maximised the number of records that could be included by constructing age models based solely on oxygen isotope data. A standardised framework was developed that allows datasets to be placed on a common chronological framework for the last 150 000 years. For this we determined the timing of δ^{18}O maxima that can be recognized in both benthic and planktonic δ^{18}O records, using the chronology of Shackleton et al. (2000), which can be readily recognized in higher resolution records. Approximately half of the benthic oxygen isotope signal results from changes in sea-level that affect benthic δ^{18}O synchronously to within the mixing timescale of the ocean. Therefore, δ^{18}O maxima approximate to sea level minima (Shackleton et al., 2000). The ages of δ^{18}O maxima – 18, 62, 87, 108 and 137 ka – are compatible with the ages of analogous events at Dome Fuji on a timescale based on the O_2/N_2 ratio of gas trapped in the ice-core (Kawamura et al., 2007), which has 2σ absolute age uncertainties of approximately 1000–2500 years. Dates between δ^{18}O maxima were estimated by applying uniform sedimentation rates between δ^{18}O maxima. The resulting δ^{18}O timeseries, filtered by the same method as δ^{13}C data (described in Sect. 3.1.1) are plotted in Fig. 3, as anomalies relative to the LGM.

δ^{18}O maxima were initially treated as synchronous throughout the ocean, despite known asynchroneities in climate events expected to distort the δ^{18}O signal. Asynchroneities of 1.5–3 ka have been identified between the Northern and Southern ice sheets (Blunier and Brooks, 2001). Using ^{14}C dating, Skinner and Shackleton (2005) and Labeyrie et al. (2005) obtained Atlantic-Pacific leads of 3.9 and 1.5 ka, respectively, for the most rapid decrease in δ^{18}O during deglaciation, and Labeyrie et al. (2005) obtained large asynchroneities between intermediate and deep waters within the Atlantic basin. Due to the sparsity of ^{14}C records, and their inapplicability to the 62, 87, 108, and 137 ka δ^{18}O maxima, systematic regional changes to the age models were not made. Moreover, both the Skinner and Shackleton (2005) and Labeyrie et al. (2005) studies, δ^{18}O maxima from all records were within 2000 years of 18 ka, which we show to be small compared with other likely errors in the age models.

We now provide an estimate of the age error associated with our approach and discuss proposed improvements. Age errors in individual records could be reduced using additional stratigraphic constraints or age control points from ^{14}C data or tephra layers. However, such data were not available for most records, and to introduce heterogeneity to the synthesis by applying a mixture of methods would likely increase the relative age errors between cores. Instead, we estimate the

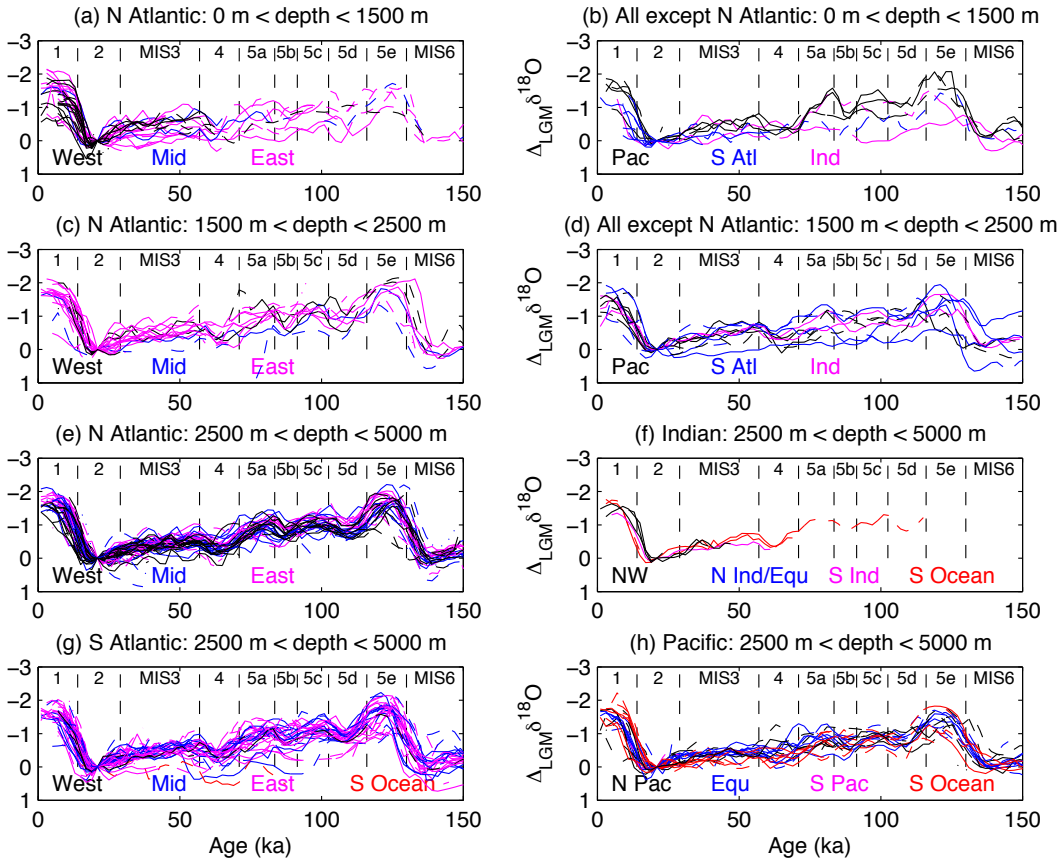

Fig. 3. Benthic δ^{18}O, as an anomaly relative to the 21 ka value, time-series by region. Timeseries are smoothed by the method described in Sect. 3.1.1, and data with a temporal resolution poorer than 6 ka removed, but no species corrections or error estimates are made. In a small number of records, the δ^{18}O maxima (note the reversed δ^{18}O axis) differ from 18, 62, 87, 108, and 137 ka; these occur either where there is disagreement regarding the timing of the δ^{18}O maxima in records from different species from the same core, or where not all δ^{18}O maxima could be identified with confidence. Marine Isotope Stages are indicated in each panel.

error associated with our age modelling approach by comparing our age estimates with previously published age models for the 116 cores for which these were available with the raw data (see Table 1 for references). Figure 4 shows the distribution of offsets of our age estimates from previous age estimates. For each of the four ocean basins considered, the age models agree to within 6 ka for approximately 95% of observations. Since there are more observations from high resolution records, this result is biased towards such records, whereas greater errors might be expected in low resolution records. Giving each record equal weight by normalising by the record length, 93% of observations agree to within 6 ka. The distribution is approximately gaussian, with no clear bias towards underestimating or overestimating age in any basin. This is also true if the previous age estimates used are restricted to those based on ^{14}C measurements (plotted in bold in Fig. 2). In Sect. 4.4 we show that applying regionally uniform adjustments to our age model in order to minimise the age error in records with ^{14}C derived age models has negligible effect on our results, and therefore we persist with the initial approach of treating δ^{18}O maxima as synchronous.

In ascribing age uncertainties, we note that disagreement between two age models may indicate error in either age model, and may be associated with the error in the absolute age scale rather than in the relative ages of records, suggesting that it would be pessimistic to equate the difference between the two age estimates with the error in our age estimates. On the other hand, errors common to our age estimates and previously published estimates are possible where ^{14}C data were not used in constructing either age model (for example, asynchroneities between δ^{18}O signals are likely to affect orbitally tuned age models similarly to our age model). We ascribe a 2σ error of 6 ka throughout most of the dataset, slightly greater than the error of 5 ka attributed to age models obtained by orbitally tuning of several proxies by Martinson et al. (1987). Errors are much smaller between the LGM and the Holocene, and typically greatest during Marine Isotope Stage (MIS) 3 (29–57 ka), which we attribute

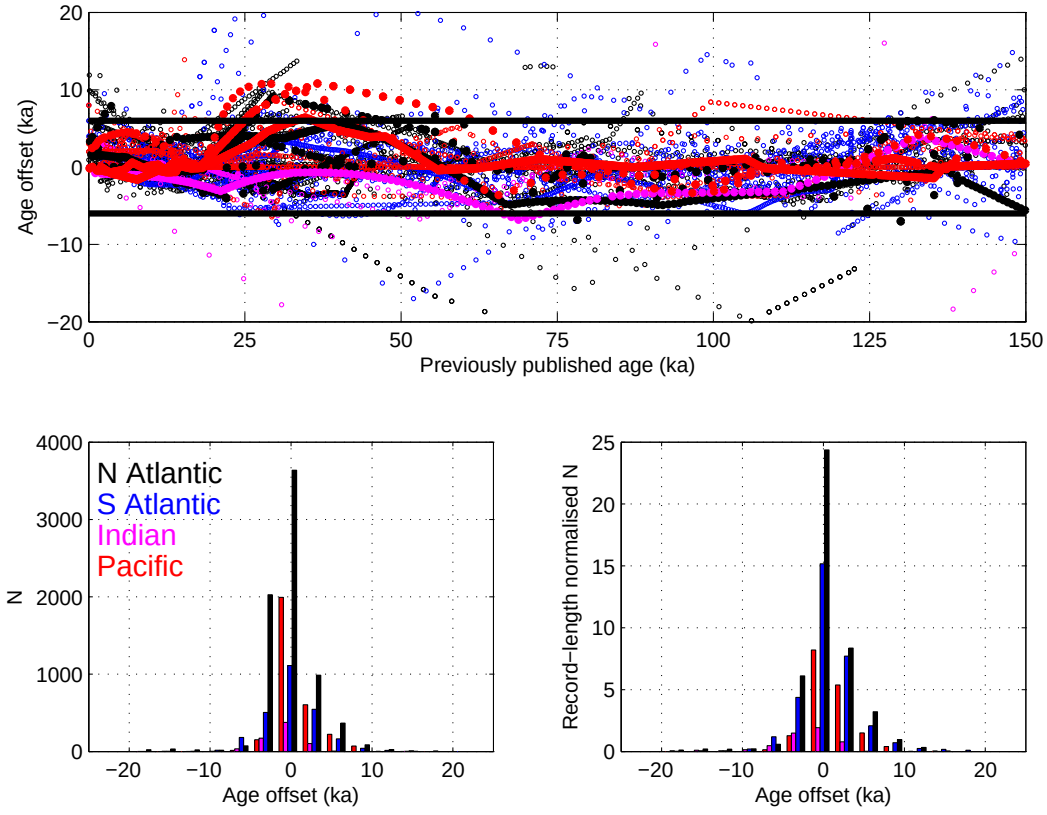

Fig. 4. (a) Offsets between age estimates used for this study and previously published (Table 1) age estimates as a function of age. Colours indicate ocean basin; bold filled circles indicate that ^{14}C data was used in the previously published age model (note that ^{14}C can only be used to improve age estimates for the last ∼50 ka). The bold black line indicates offsets of ±6 ka. **(b)** Distribution of age estimate offsets. **(c)** Distribution of age estimate offsets, normalised by the number of observations within each record (i.e. an observation from a record of length n adds $1/n$, as opposed to 1, to the appropriate bin).

to the large interval (between 18 and 62 ka) over which a uniform sediment accumulation rate must be assumed, and MIS 6 (>137 ka). The ascribed age error is increased to 8 ka during these MIS 3 and 6. We attribute the increased errors during MIS 3 to the long interval between δ^{18}O maxima (44 ka), which would be expected to increase errors due to non-uniform sedimentation rate. We therefore emphasise that, due to the age modelling approach employed, the synthesis is not suitable for examining the phasing of climate events between ocean basins, nor millennial timescale variations in δ^{13}C.

3 Procedure for temporal gridding and δ^{13}C uncertainty estimation

This section describes the treatment of data inhomogeneity within and between records in obtaining a temporally gridded data synthesis, with uncertainties ascribed to individual δ^{13}C values as a function of species, core location, data resolution and scatter. In accounting for data inhomogeneities, it is useful to distinguish between systematic errors associated with each record (inter-record error) and the temporally varying error component (intra-record error). For example, the error due to fractionation during calcification has a large inter-record component because this is strongly dependent on species, and most records consist of samples from a single species or genus. Spatial variability in the species offset is also an inter-record error, but in situ variability of this offset in response to climate change is an intra-record error. Similarly, any systematic difference in δ^{13}C resulting from inter-laboratory calibration errors is an inter-record error. Since we expect uncertainties in the systematic inter-record error to be significant, δ^{13}C and its uncertainties are estimated by two stages. First, we present intra-record variability in δ^{13}C relative to the LGM, which we label $\Delta_{\mathrm{LGM}}\delta^{13}$C (Sect. 3.1). Second, we obtain estimates for absolute δ^{13}C values (Sect. 3.2). $\Delta_{\mathrm{LGM}}\delta^{13}$C can be used to understand spatial patterns of δ^{13}C variability, and

has smaller uncertainty than absolute δ^{13}C. Therefore, we recommend that $\Delta_{\rm LGM}\delta^{13}$C is chosen where possible when using this data synthesis (for example for model-data comparison), and it is also the variable presented in most figures within this paper.

3.1 Obtaining δ^{13}C as anomalies relative to the LGM

A smoothing spline, approximating a 10 ka low pass filter (Sect. 3.1.1), was applied to the data, removing high frequency variability such as Dansgaard-Oeschger oscillations which are beyond the precision of the age model. All $\Delta_{\rm LGM}\delta^{13}$C values are calculated as an anomaly relative to the LGM. This is defined at 21 ka, providing a good approximation to the LGM definition of 19–23 ka (e.g. Mix et al., 2001); averaging pre-processed data within the 19–23 ka interval would not be preferable due to uncertainties in the age model. The LGM, rather than the late Holocene, is chosen as the reference period because almost all cores provide LGM data, whereas approximately half of all cores provide no data for < 4 ka.

Three steps were taken to obtain $\Delta_{\rm LGM}\delta^{13}$C estimates and uncertainties, described in detail below. First, each time-series was smoothed and gridded, and the error associated with this process estimated (Sect. 3.1.1). Second, an additional error was estimated for cores thought to be subject to changes in the phyto-detritus effect (Sect. 3.1.2). Third, an error for the representativeness of each species of the ambient water was estimated (Sect. 3.1.3). Although the errors associated with each of these steps are likely to be correlated, there were insufficient data to reliably estimate these correlations, so the total error was estimated to be the quadratic sum of the error components. 2σ error estimates are quoted; where they exceed 1‰ or where the data resolution is poorer than 6 ka, no final $\Delta_{\rm LGM}\delta^{13}$C estimate is given. Full error estimates are provided as part of the uniformly spaced output dataset (Supplementary Materials). Data are output on a 2-ka grid as an aid to visualisation, but note that the age error estimates are of 6–8 ka.

3.1.1 Smoothing splines

The first step in obtaining $\Delta_{\rm LGM}\delta^{13}$C estimates was independent of species or region, and a function only of the input time-series data. These were smoothed and placed on a uniform 2 ka grid using the spline smoothing method described by Silverman (1985). For a time-series of n observations, the set of $n-1$ cubic equations was obtained which minimised

$$\theta = \lambda \int_{t_1}^{t_n} \ddot{y}^2 \mathrm{d}t + n^{-1} \Sigma_{i=1}^{n} y_i'^2, \tag{1}$$

where λ is the smoothing parameter, y is the output δ^{13}C estimate and $\ddot{y}$ is its second derivative with respect to time, t_1 and t_n are dates for the top and bottom, respectively, of each record (note that t is defined positive towards the past), and y' is given by

$$\begin{aligned} y_i'^2 &= (y_i - Y_i)^2, & |\, y_i - Y_i \,| &\leq y_{\rm thr}, \\ y_i'^2 &= y_{\rm thr}^2 + |\, y_i - Y_i \,| - y_{\rm thr}, & |\, y_i - Y_i \,| &> y_{\rm thr}, \end{aligned} \tag{2}$$

where Y_i is the δ^{13}C observation and $y_{\rm thr} = 0.5$‰ was chosen to prevent outliers from having a dominant effect on the estimate (Enting, 1987). The smoothing parameter is given by

$$\lambda = \frac{(n-1)T_{0.5}^4}{(2\pi)^4 (t_n - t_1)}, \tag{3}$$

where $T_{0.5}$ was chosen to be 10 ka. For a uniformly spaced input time-series, this method is equivalent to a kernel filter admitting 50% of variability with a period of $T_{0.5}$, steeply increasing towards 100% at longer timescales and steeply decreasing towards 0% at shorter timescales (Enting, 1987). For time-series with non-uniformly spaced data, the period at which 50% of the variability is admitted is a weak function ($\sim \hat{f}^{-\frac{1}{4}}$) of the local kernel density $\hat{f}$. Kernel data density estimates, which approximate to the inverse of the temporally local data resolution Δt, are provided as part of the uniformly spaced output dataset (Supplementary Materials).

A first estimate of the error in the smoothed time-series is given by (Silverman, 1985)

$$2\sigma_{\rm sil}(t) = 2\left(4\lambda^{\frac{1}{3}} \hat{f}(t)\right)^{-\frac{3}{8}} \left(\frac{\Sigma_{i=1}^{n} y_i'^2}{n^{\frac{3}{4}} - 2^{-\frac{3}{2}} \lambda^{-\frac{1}{4}} \Sigma_{i=1}^{n} \hat{f}(t_i)} \right)^{\frac{1}{2}}. \tag{4}$$

Typical values of $2\sigma_{\rm sil}$ are of the order of 0.1‰, rarely increasing above 0.25‰. However, this method is intended for time-series with large n, and unrealistically small error estimates are produced for time-series with a temporal resolution of the same order as $T_{0.5}$. Enting (1987) noted that an accurate error estimate depends on a knowledge of the spectral

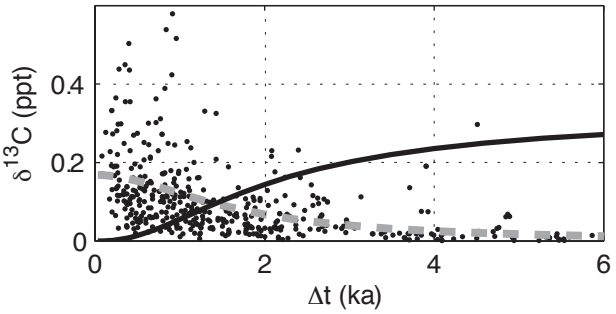

Fig. 5. Estimate of aliasing error, $2\sigma_{\rm ali}$, as a function of data resolution Δt (solid line). Dots are the root-mean-square of the residuals for each record, y', as a function of mean data resolution, with a line of best fit, y'_h (dashed line). $2\sigma_{\rm ali}$ is calculated using Eq. (5).

characteristics of both the signal and the noise. For our purposes, all high frequency variability is noise, and it is likely that this is aliased in low resolution time-series. In order to address this, we assume that the root-mean-square of the residuals, $\bar{y'}$, from high resolution time-series provides an estimate of the noise present in all time-series. Where smaller values of $\bar{y'}$ are obtained from low resolution records, this indicates that variability in the high frequency ($T < T_{0.5}$) band is being aliased as a signal at lower frequencies. $\bar{y'}$ is plotted as a function of time-series mean resolution in Fig. 5, along with a line of best fit, y'_h, with the form of a *tanh* function. We obtain lower values of y'_h in low resolution cores. The resulting error estimate due to aliasing,

$$2\sigma_{\mathrm{ali}}(\Delta t) = 2\left(y'_h(0) - y'_h(\Delta t)\right)\left(1+\frac{T_0}{\pi\,\Delta t}\right)^{-\frac{1}{2}}, \quad (5)$$

is also plotted in Fig. 5. Note that there is a large range in y'_h even within high frequency time-series, likely to be largely caused by data inhomogeneities about which information is often unavailable (e.g. shell sizes used; shells per sample; averaging of duplicate samples). Therefore aliasing error estimates for low resolution time-series are very uncertain. The total error associated with the smoothing spline process is the quadratic sum of $2\sigma_{\mathrm{sil}}$ and $2\sigma_{\mathrm{ali}}$.

3.1.2 Error due to the phyto-detritus effect

A further source of error is the possible change in time of the depositional environment in which benthic foraminifera exist. Infaunal species such as those in the *Uvigerina* genus inhabit a microenvironment that is often depleted in δ^{13}C due to the respiration of organic matter in the sediment, whereas epifaunal species are not typically subject to this effect. There is some evidence that the offset in infaunal species varies over a glacial cycle (Hoogakker et al., 2010), but there are insufficient data to determine a correction that varies over time. In this study, we treat this effect as a constant component of the species offset plus a random error (Sect. 3.1.3); therefore there is no phyto-detritus correction to $\Delta_{\mathrm{LGM}}\delta^{13}$C in infaunal species.

Although shells from the epifaunal *Cibicidoides* taxon are thought usually to record the δ^{13}C of ambient water ΣCO_2 accurately, several studies have identified a bias toward low values in high productivity regions (Mackensen et al., 1993; Sarnthein et al., 1994), termed the phyto-detritus effect. Bickert and Wefer (1999) compared cores from upwelling regions in the Atlantic Ocean to nearby cores outside upwelling regions and found that δ^{13}C in upwelling regions was more depressed, relative to nearby cores, during the LGM than the late Holocene. Bickert and Mackensen (2003) applied a correction of +0.4‰ to LGM δ^{13}C in several upwelling regions in the Atlantic Ocean (parts of the eastern boundary in both hemispheres; equator; subtropical and subantarctic fronts), applying no analogous correction to Holocene values. Such a time-dependent correction would influence both δ^{13}C and $\Delta_{\mathrm{LGM}}\delta^{13}$C estimates. However, the temporal and spatial structure of such a correction is poorly understood. Instead, we add a $2\sigma_{\mathrm{phy}}$ error of 0.4‰ to the records upwelling regions where phytodetritus errors are more likely (flagged in Table 1). In Sect. 4.4 we investigate whether a bias is introduced to the data synthesis by not applying a phytodetritus correction.

It is not well known to what extent the phyto-detritus effect in epifaunal species is caused by changes in foraminifer growth rate (McConnaughey et al., 1997), or by the build-up of respiring organic matter over epifaunal species leading to a decrease in δ^{13}C, similar to that observed in infaunal species. No correlation has been observed between sedimentation rate and amplitude of the phyto-detritus effect, although Mackensen et al. (2001) suggested that this is because the key control is seasonal peak deposition rate, rather than annual mean deposition rate. It is therefore uncertain whether additional errors are introduced to records from infaunal species in high productivity regions. As noted above, we apply no correction, but add the same uncertainty as would be added to epifaunal species.

3.1.3 Disequilibria and the calculation of species errors

An important error in $\Delta_{\mathrm{LGM}}\delta^{13}$C estimates is variability in disequilibria of δ^{13}C in calcium carbonate in the shells of foraminifera, relative to the ambient water. Along with the phyto-detritus effect, δ^{13}C disequilibrium leads to the application of different "species offsets" to δ^{13}C data collected from different species. We note that $\Delta_{\mathrm{LGM}}\delta^{13}$C is independent of any uniform species offset, and that errors due to variability between individual shells, or small groups of shells, of a given species have already been implicitly accounted for in the smoothing spline calculation. Of interest here are the causes of variability in the disequilibrium of calcium carbonate through time.

In planktonic formanifiera, recorded δ^{13}C is a strong function of shell size (e.g. Berger et al., 1978; Spero and Lea, 1993; Elderfield et al., 2002), and the difference in δ^{13}C between the largest and smallest size fractions can be greater than glacial-interglacial differences of the order of 0.5‰ (Oppo and Fairbanks, 1989). Therefore, δ^{13}C measurements from both planktonic and benthic species are usually made on shells selected for size fraction. Nevertheless, any unrecorded changes in shell size throughout a record may lead to significant error in $\Delta_{\mathrm{LGM}}\delta^{13}$C. A second source of error is temperature-dependent fractionation, which affects planktonic species due to variability in surface temperature on seasonal to glacial timescales. The temperature-dependence of fractionation is a function of species. Culture experiment estimates of $\partial(\delta^{13}C)/\partial(T)$ (where T is temperature) have been made of -0.11‰ $^{\circ}C^{-1}$ for *Globigerina bulloides* (Bemis et al., 2000), -0.08‰$^{\circ}C^{-1}$ for *Limacina inflata* (Fischer et al., 1999), 0 to $+0.05$‰ $^{\circ}C^{-1}$ for *Orbulina universa* (Bemis et al., 2000). No relationship with temperature was

Table 2. Species-specific error estimates and uniform adjustments applied to the dataset. Correction and correction error estimates affect the calculation of δ^{13}C but not $\Delta_{\mathrm{LGM}}\delta^{13}$C; where no correction is given, no absolute δ^{13}C estimate is made.

Species	$\Delta_{\mathrm{LGM}}\delta^{13}$C error, ‰	Correction, ‰	Correction error, ‰
C. wuellerstorfi	0.15	0	0.20
Benthics			
Other *Cibicidoides*	0.35	0	0.28
Uvigerina spp.	0.23	+0.85	0.48
H. elegans or unspecified	0.6	–	–
Other benthic spp.	0.4	–	–
Planktonics			
G. ruber	0.4	0	0.2
G. bulloides	0.4	+2.11	0.32
G. sacculifer	0.4	-0.27	0.2
N. pachyderma	0.4	+0.68	0.39
Other planktonic spp.	0.6	–	–

observed on *Globigerinoides ruber* (Fischer et al., 1999), whereas Kohfeld et al. (2000) assumed a relationship of -0.13‰ °C^{-1} for *Neogloboquadrina pachyderma*.

Culture experiments on planktonic foraminifera also reveal a strong dependence on the concentration of the carbonate ion, with a gradient of approximately -0.012‰/(µmol kg^{-1}) for *G. bulloides* under constant DIC (Spero et al., 1997). Glacial carbonate concentration is dependent on the poorly constrained alkalinity inventory of the ocean, but a change of 30 to 80 µmol kg^{-1} is not implausible (Kohfeld et al., 2000), indicating an effect of the same order as glacial δ^{13}C cycles. The effect of carbonate ion on benthic δ^{13}C is not known. Increases in light availability have been found to increase δ^{13}C in *Globigerinoides sacculifer*, leading Spero and Lea (1993) to propose that the correlation between shell size and δ^{13}C is principally caused by the dependence of both growth rate and δ^{13}C on ambient light levels. Further effects arise due to changes in the isotopic composition of carbon in the diet. Culture experiments indicate that δ^{13}C in *G. bulloides* shell carbonate varies as δ^{13}C in organic matter in the ratio 0.084:1 (Spero and Lea, 1996). Finally, the planktonic δ^{13}C signal can be distorted from a surface signal by secondary calcification in deeper, typically isotopically lighter, waters, as observed by Duplessy et al. (1981b) on *G. sacculifer* transferred to laboratory tanks.

With the exception of sea-surface temperature reconstructions for the LGM (e.g. MARGO Project Members, 2009), variability in water properties likely to cause systematic errors in $\Delta_{\mathrm{LGM}}\delta^{13}$C are poorly constrained over the last 150 ka, so no time-varying correction is applied to $\Delta_{\mathrm{LGM}}\delta^{13}$C. Therefore, we caution that changes in these properties over a glacial cycle, rather than changes in seawater δ^{13}C, may contribute significantly to variability in the planktonic $\Delta_{\mathrm{LGM}}\delta^{13}$C record. However, Earth system models that output δ^{13}C can also produce temperature, alkalinity and pH fields, so that this is not an obstacle to model-data comparison; the validity of such comparisons are instead limited by the general applicability of the above empirical relationships. Moreover, we note that these caveats are a much lesser concern when interpreting the benthic δ^{13}C record.

A random error estimate may be made by comparing records from different species but from the same core. Among benthic species, the epibenthic taxon *Cibicidoides wuellerstorfi* is widely preferred for recording δ^{13}C, and to this species we ascribe an error of 0.15‰. This value is obtained from comparison of water column data (Kroopnick, 1985) with data from core samples (c.f. Beveridge et al., 1995). Error estimates for other species in the *Cibicidoides* genus were obtained using cores containing both *C. wuellerstorfi* and another *Cibicidoides* species. The error is the root-mean-squared (rms) difference between the two species after the application of an optimal species offset. This process was repeated for the infaunal genus *Uvigerina*. For other species, there was insufficient overlap in data with *C. wuellerstorfi* to apply this method. For these species, errors of 0.4‰ were ascribed. A larger error of 0.6‰ was applied to data derived from *Hoeglandia elegans* or from mixed benthics. Error estimates are presented in Table 2.

For planktonic foraminifera, the choice of reference species is less clear. We select *G. ruber*, which yields data that are consistent on a regional scale, and has a restricted depth range (Fischer et al., 1999), so that changes in recorded δ^{13}C are more likely to reflect changes in surface conditions. We ascribe an error of 0.4‰ to this species, and calculated estimates for *G. bulloides*, *Globigerinoides sacculifer*, and *N. pachyderma* by the same method used for benthic species. However, since these relative errors are less than 0.4‰, we ascribe an error of 0.4‰ to each of these species. These are presented in Table 2. We ascribe an error of 0.6‰ to other planktonic species.

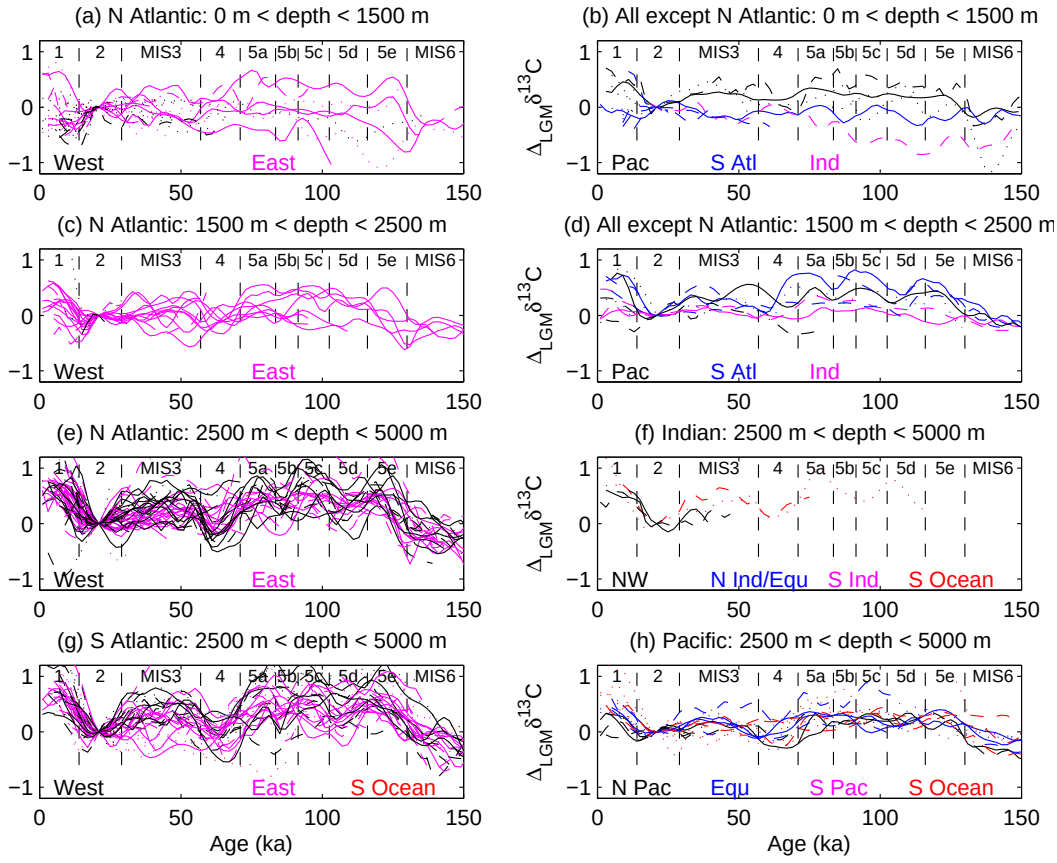

Fig. 6. Benthic $\Delta_{LGM}\delta^{13}C$ ($\delta^{13}C$ as an anomaly relative to the 21 ka value) time-series by region. Error estimates are <0.25‰ (solid), <0.5‰ (dashed), <0.8‰ (dotted); data with larger error estimates are not plotted. Colours indicate sub-regions: meridional boundaries are at the mid-ocean ridge (Atlantic) and 75°E (Indian). Equatorial cores are within 8°of the Equator. Marine Isotope Stages are indicated in each panel.

3.2 Obtaining absolute δ^{13}C values

Absolute δ^{13}C values within each time-series are the sum of $\Delta_{LGM}\delta^{13}$C estimates and the LGM δ^{13}C value. The LGM δ^{13}C estimate is the value output from spline smoothing plus a species-specific uniform correction. For the benthic genus *Cibicidoides* and the planktonic species *G. ruber*, we ascribe a correction of 0 ± 0.2‰. The correction and correction error for other species are obtained by calculating the mean and standard deviation of the offsets used to optimise the least-squares-fit between different species in the same core, as described in Sect. 3.1.3. This precludes any spatial variability in the species offset, because despite evidence that these offsets change over a glacial cycle (Hoogakker et al., 2010), there are insufficient data to quantify this variability globally. We obtain a correction of $+0.85 \pm 0.48$‰ for *Uvigerina* species, similar to the canonical value of +0.9‰ (Shackleton and Hall, 1984). Other estimates are given in Table 2; where no correction is quoted, no absolute δ^{13}C estimate is made.

4 δ^{13}C data presentation and interpretation

For the purpose of visualisation, data were sorted into the principal regions: North Atlantic, South Atlantic, Indian Ocean and Pacific Ocean (Table 1), with subcategories for regions such as the Arctic Ocean, the Nordic Seas, and the South China Sea, and the Southern Ocean sector of each ocean, for which a highly inclusive definition of south of 40°S is used. By compiling all available δ^{13}C data in each region, presented as an anomaly relative to the LGM, and plotting on a uniform timescale, we can look for large scale changes in δ^{13}C that might be obscured or biased by consideration of a small number of cores. Nevertheless, there are sampling biases towards coastal areas in each ocean, towards the eastern Atlantic and towards the Arabian Sea in the Indian Ocean (Fig. 2), as well as towards the 2500–3500 m depth range. Data coverage is insufficient to interpolate and extrapolate in three dimensions, but estimates might be refined with new data or by dynamical smoothing using an Earth system model.

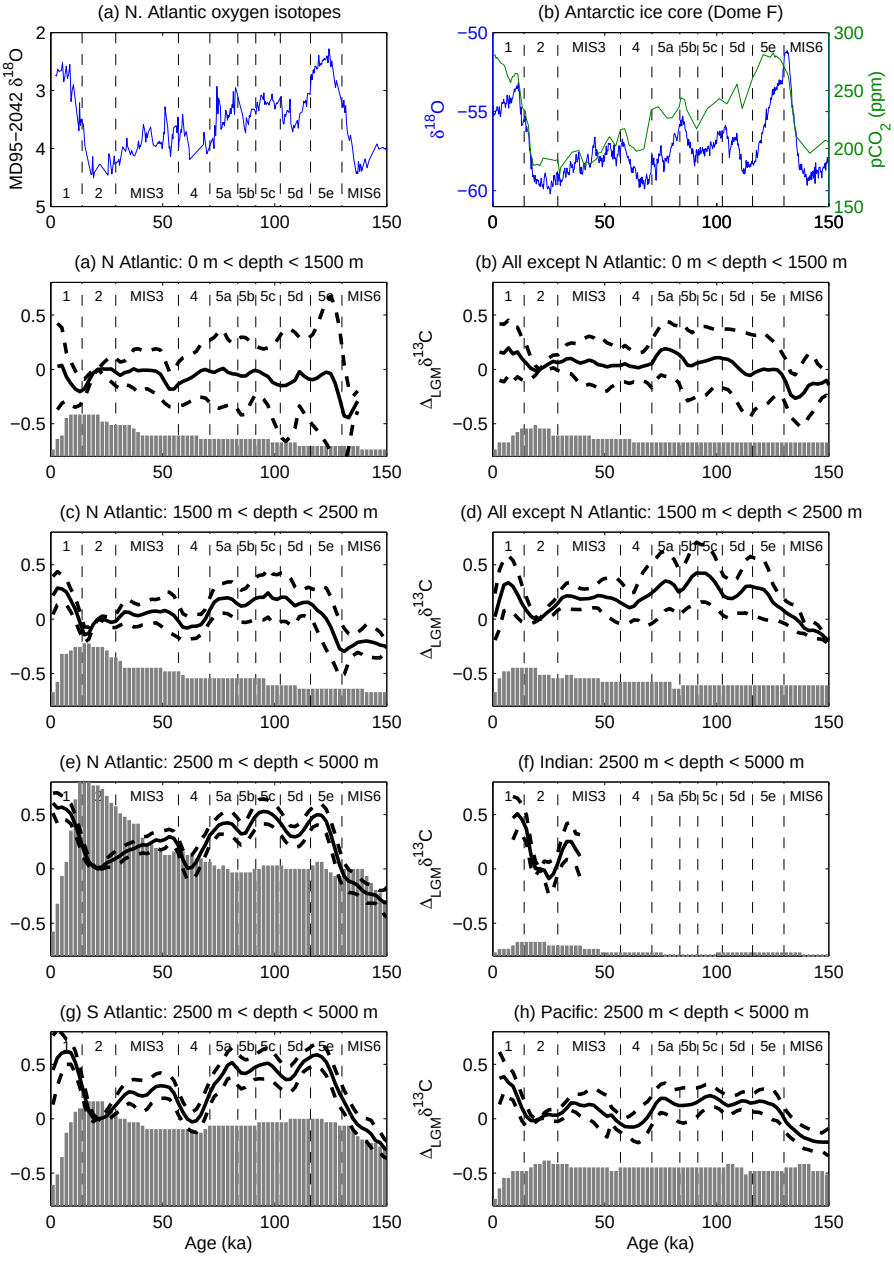

Fig. 7. Mean and 2× standard error, weighted by the square of the inverse of the error estimate, of benthic $\Delta_{LGM}\delta^{13}$C in each region. The histogram indicates the number of records used; where this is fewer than three, no data are plotted. Panel **(a)** shows δ^{18}O from core MD95-2042 in the North Atlantic (37.8° N; 10.2° E; 3146 m). Panel **(b)** shows CO_2 and δ^{18}O from the Dome Fuji ice core (Kawamura et al., 2007); note that the age model used in this study is based on the Kawamura et al. (2007) timescale.

4.1 Benthic time-series

In Fig. 6 we present $\Delta_{LGM}\delta^{13}$C time-series grouped by region, excluding all data from the Arctic Ocean or from marginal seas (except the South China Sea), and by depth. Only where the temporal resolution of the pre-processed data was sufficiently high ($\Delta t < 6$ ka) and the estimated error sufficiently low (<0.8‰) are data plotted. The mean and 2× standard error of data from each region were calculated and are plotted in Fig. 7. Sampling biases towards ocean boundaries, and towards regions with high sedimentation rates, are not removed in the averaging calculation. Therefore Fig. 7 is not an unbiased estimate of regional averages, but rather an estimate of $\Delta_{LGM}\delta^{13}$C where data exist within each region.

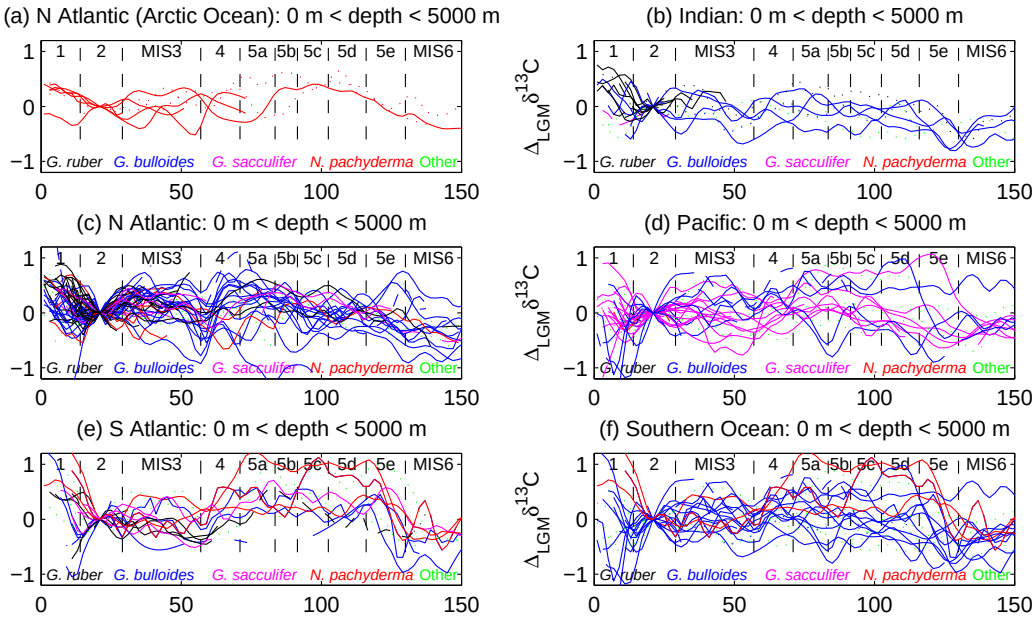

Fig. 8. Planktonic $\Delta_{LGM}\delta^{13}$C time-series by region. Error estimates are <0.5‰ (solid), <0.6‰ (dashed), <0.8‰ (dotted); data with larger error estimates are not plotted (note these thresholds are different from thresholds for benthic data). Colours indicate planktonic species: *G. ruber* (black); *G. bulloides* (blue); *G. sacculifer* (magenta); *N. pachyderma* (red); other (green).

In waters deeper than 2500 m, a consistent pattern is observed within the North Atlantic, South Atlantic, and Pacific Oceans. These basins exhibit maxima in δ^{13}C during temperature maxima, with small differences between the Eemian interglacial (MIS 5e), the MIS 5c and MIS 5a interstadials, and the Holocene (MIS 1). MIS 4 and MIS 6 are marked by values of δ^{13}C similar to or lower than LGM values, consistent with a longer timescale trend towards higher δ^{13}C (Hoogakker et al., 2006). The principal difference between the basins is in the amplitude of δ^{13}C variations. The North Atlantic exhibits slightly larger amplitude changes in δ^{13}C than the South Atlantic. The amplitude of the glacial cycle in the Pacific basin is approximately half that in the Atlantic basin. Furthermore, there is much less variability observed in the Pacific at around precessional timescales; MIS 3 is a much weaker peak, whereas troughs during MIS 5b and MIS 5d are not consistently recorded. Typically lower sedimentation rates in the Pacific, leading to poorer data resolution, may contribute to the latter result. Another bias may arise from a weak positive correlation between bathymetric depth and the amplitude of variability. However, the mean depth of >2500 m cores in the Pacific (3400 m) is only slightly shallower than that in the Atlantic (3600 m), so this can explain less than 0.05‰ of the difference between the two basins. The lack of long records from deeper than 2500 m in the Indian Ocean prevent us from concluding whether there is similar variability in δ^{13}C over a full glacial cycle, although the amplitude of change between the LGM and the Holocene is greater than typical Pacific but smaller than typical Atlantic amplitudes.

Much of the variability in deep $\Delta_{LGM}\delta^{13}$C is likely to arise from changes in the global ocean δ^{13}C reservoir, influenced by the storage of isotopically light carbon in the biosphere. This is supported by the qualitative similarity between the Pacific and the Atlantic $\Delta_{LGM}\delta^{13}$C, unless there are changes of the opposite sign within intermediate or pycnocline waters. There is some evidence, from Pacific cores in the 1500–2500 m depth range, for such changes over the time interval since the LGM (c.f. Duplessy et al., 1988b). However, records from a similar depth in the Indian Ocean, as well as shallower Pacific records, present a pattern that is broadly consistent with that observed in the deep Pacific.

Glacial variations in intermediate and pycnocline Atlantic δ^{13}C are thought to be strongly influenced by changes in the depth and range of the Atlantic overturning cell, in competition with Antarctic Bottom Water and Antarctic Intermediate Water, although changes in the partitioning of remineralised carbon have also been invoked (Boyle, 1988). Here, we note that Atlantic $\Delta_{LGM}\delta^{13}$C in the 1500–2500 m depth range is similar to that observed in the Indian Ocean at the same depth, and in the deep Pacific Ocean. An exception is during deglaciations, when there are lower values of Atlantic intermediate water $\Delta_{LGM}\delta^{13}$C. Holocene $\Delta_{LGM}\delta^{13}$C in <1500 m deep cores is usually negative, particularly in the West Atlantic, whereas there is no consistent pattern prior to the LGM.

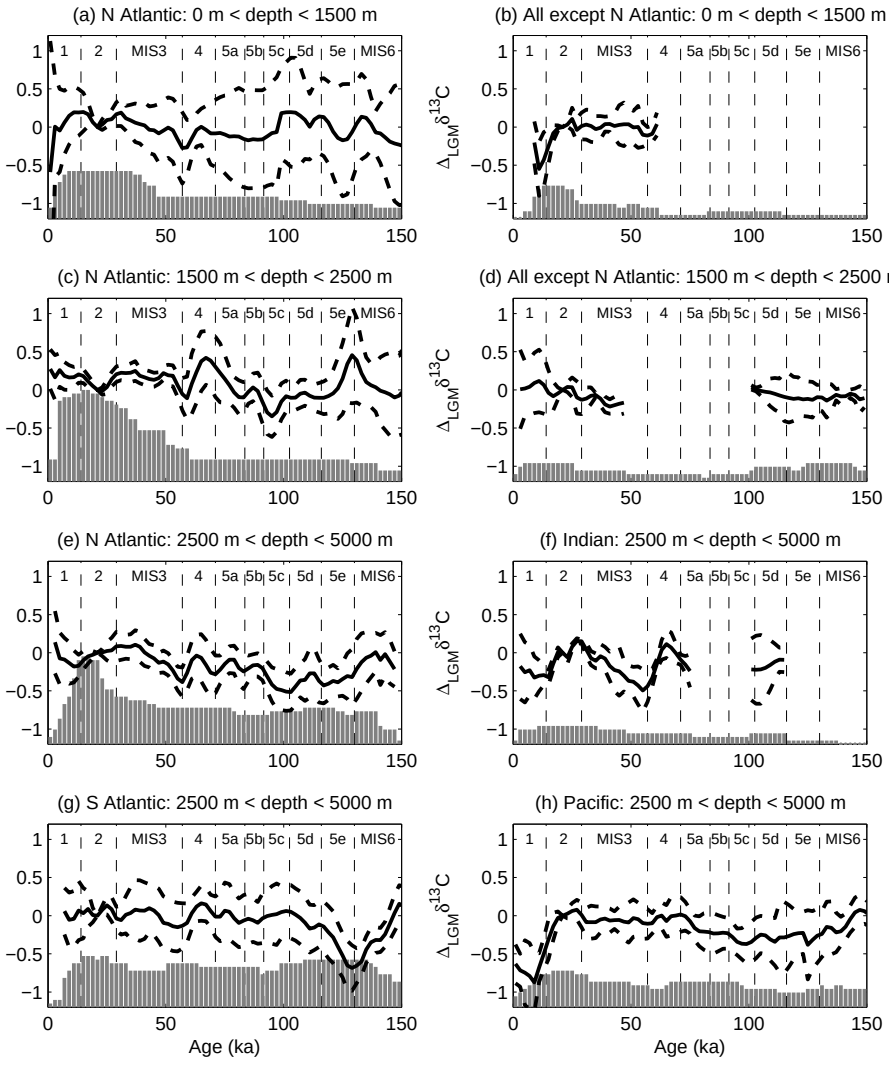

Fig. 9. Mean and 2× standard error, weighted by the square of the inverse of the error estimate, of planktonic minus benthic $\Delta_{LGM}\delta^{13}C$ ($\Delta_{LGM}\delta^{13}C_{p-b}$)in each region. Note that $\Delta_{LGM}\delta^{13}C_{p-b}$ was calculated for each record prior to averaging.

4.2 Planktonic time-series and planktonic/benthic differences

Planktonic $\Delta_{LGM}\delta^{13}C$ time-series, grouped by region, are presented in Fig. 8. There is less agreement between different planktonic records within a region, compared to benthic records, consistent with the large uncertainty attributed to the estimation of seawater $\Delta_{LGM}\delta^{13}C$ from planktonic species (Sect. 3.1.3). *G. ruber* records from the North Atlantic and Indian Oceans consistently show elevated Holocene $\Delta_{LGM}\delta^{13}C$ values. Temperature maxima also exhibit higher $\Delta_{LGM}\delta^{13}C$ values than temperature minima in most *G. bulloides* records, although these changes are rarely outside the formal uncertainty limits. Notable exceptions are three cores from the Pacific sector of the Southern Ocean, in which low early Holocene $\Delta_{LGM}\delta^{13}C$ values are recorded, and Indian Ocean cores, which exhibit little coherent variability over 150 000 years, except for a slight upward trend. A decrease in $\Delta_{LGM}\delta^{13}C$ during MIS 4 is present in most Atlantic records but less apparent in Pacific records. There is no clear evidence for minima in planktonic $\Delta_{LGM}\delta^{13}C$ during MIS 5b and MIS 5d, in contrast to benthic records from the deep Atlantic Ocean.

The difference between $\delta^{13}C$ recorded in planktonic and benthic foraminifera has long been of interest to paleooceanographers because of its association with deep ocean carbon storage (Broecker, 1982a; Shackleton et al., 1983), although interpreting changes in seawater $\delta^{13}C$ from planktonic data is problematic (Sect. 3.1.3). The difference between planktonic and benthic $\Delta_{LGM}\delta^{13}C$, $\Delta_{LGM}\delta^{13}C_{p-b}$,

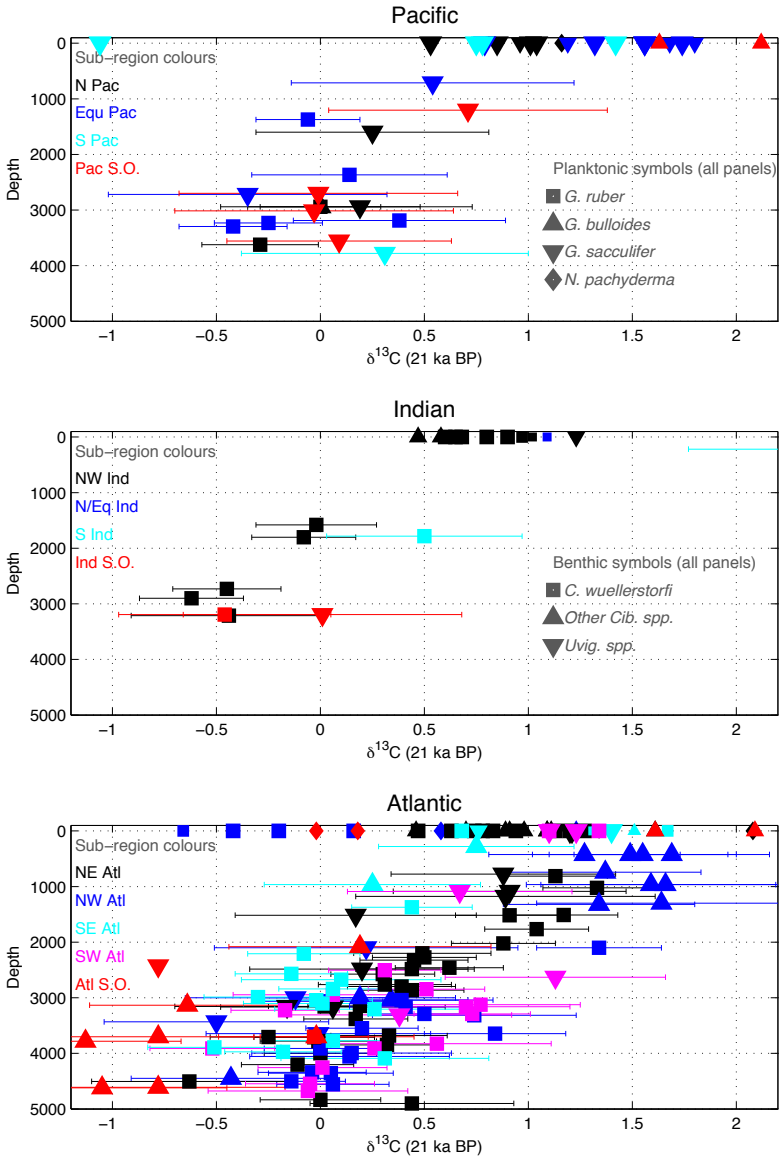

Fig. 10. 21 ka (LGM) δ^{13}C time-slice, with 2σ error bars on benthic data.

was calculated for each core where both planktonic and benthic δ^{13}C records were present. The weighted mean of $\Delta_{\mathrm{LGM}}\delta^{13}\mathrm{C}_{p-b}$ was calculated for each region and is plotted in Fig. 9 (analogous to Fig. 7). There are few benthic/planktonic pairs from the Indian Ocean, or from shallower than 2500 m in the Pacific Ocean, so that averages are constructed from 3–8 benthic/planktonic pairs in each of these regions (averages are not constructed from fewer than three pairs). Throughout all regions, $\Delta_{\mathrm{LGM}}\delta^{13}\mathrm{C}_{p-b}$ remains within two standard errors of zero for most of the 150 ka record. The most notable features occur during deglaciations (MIS 1/2 boundary; MIS 5e/6 boundary), where $\Delta_{\mathrm{LGM}}\delta^{13}\mathrm{C}_{p-b}$ is usually negative outside the North Atlantic. The very low $\Delta_{\mathrm{LGM}}\delta^{13}\mathrm{C}_{p-b}$ values obtained for MIS 1 in the Pacific are caused by anomalously low planktonic $\Delta_{\mathrm{LGM}}\delta^{13}\mathrm{C}$ in the Southern Ocean (Fig. 8); exclusion of these cores removes this feature.

Changes in the difference in δ^{13}C between surface and deep waters could be caused by changes in the relative strength of export production and meridional overturning in the global ocean. This is because the positive vertical δ^{13}C gradient, set up by the downward flux of isotopically light organic matter, is eroded by the exchange of upper ocean and deep waters. The weak δ^{13}C gradient found during deglaciations (i.e. the low value of $\Delta_{\mathrm{LGM}}\delta^{13}\mathrm{C}_{p-b}$) may indicate a decrease in export production, more rapid

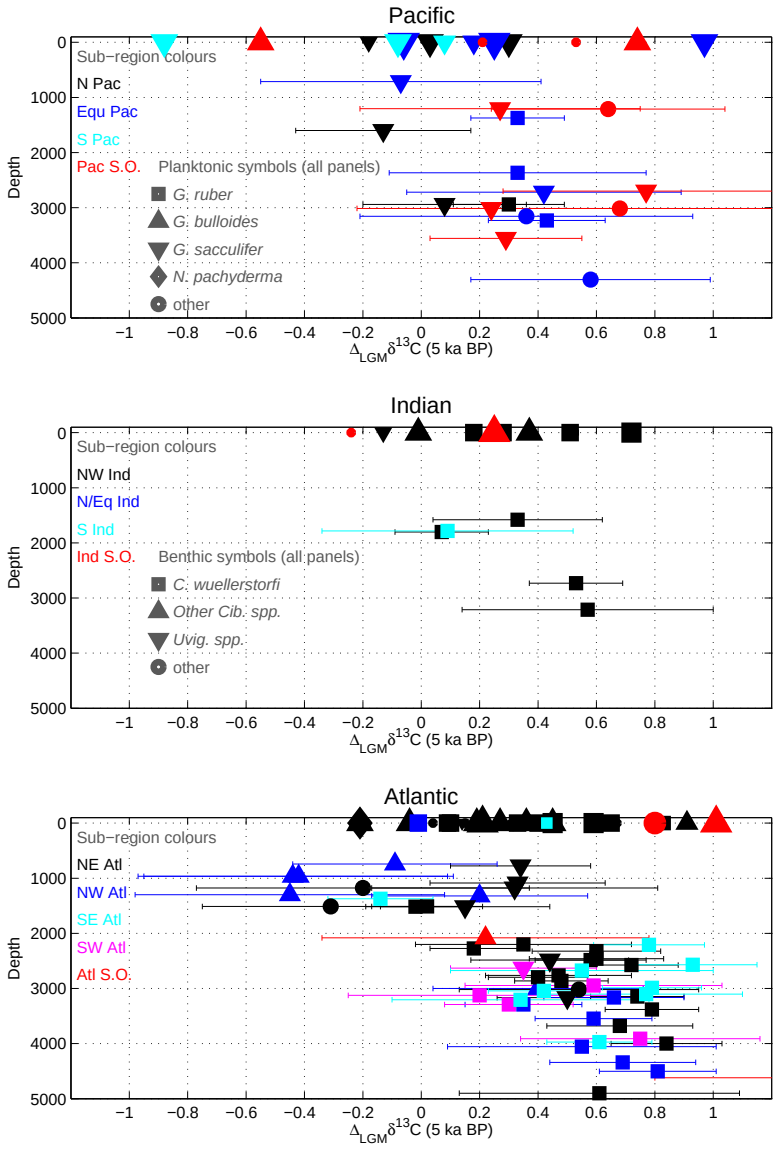

Fig. 11. 5 ka $\Delta_{LGM}\delta^{13}$C time-slice, with 2σ error bars on benthic data.

mixing between the deep and surface ocean, or a shift in downwelling towards isotopically heavier parts of the surface ocean. However, several other mechanisms influence $\Delta_{LGM}\delta^{13}C_{p-b}$, such as regional variability in productivity, circulation, and air-sea gas exchange, and periods of rapid growth or decline of the biosphere. It is also possible that variability in the $\Delta_{LGM}\delta^{13}C_{p-b}$ is dominated by variability in isotope disequilibria in planktonic foraminifera due to changes in temperature, diet, or carbonate ion concentration (Kohfeld et al., 2000).

4.3 Time-slices

A set of $\Delta_{LGM}\delta^{13}$C time-slices, as a function of depth within each ocean basin, for the Holocene (5 ka), MIS 3 (47 ka), MIS 5a (75 ka), and MIS 5e (123 ka) are plotted in Figs. 11–14. These are referenced to an absolute δ^{13}C time-slice for the LGM (21 ka), plotted in Fig. 10. We first consider the hypothesis that benthic $\Delta_{LGM}\delta^{13}$C in each time-slice is a function of ocean region and depth only, and that all deviations from the mean $\Delta_{LGM}\delta^{13}$C profile can be explained by the quoted error estimates. If the random errors are underestimated in this study, or if $\Delta_{LGM}\delta^{13}$C varies sufficiently between different water masses at the same depth in the same

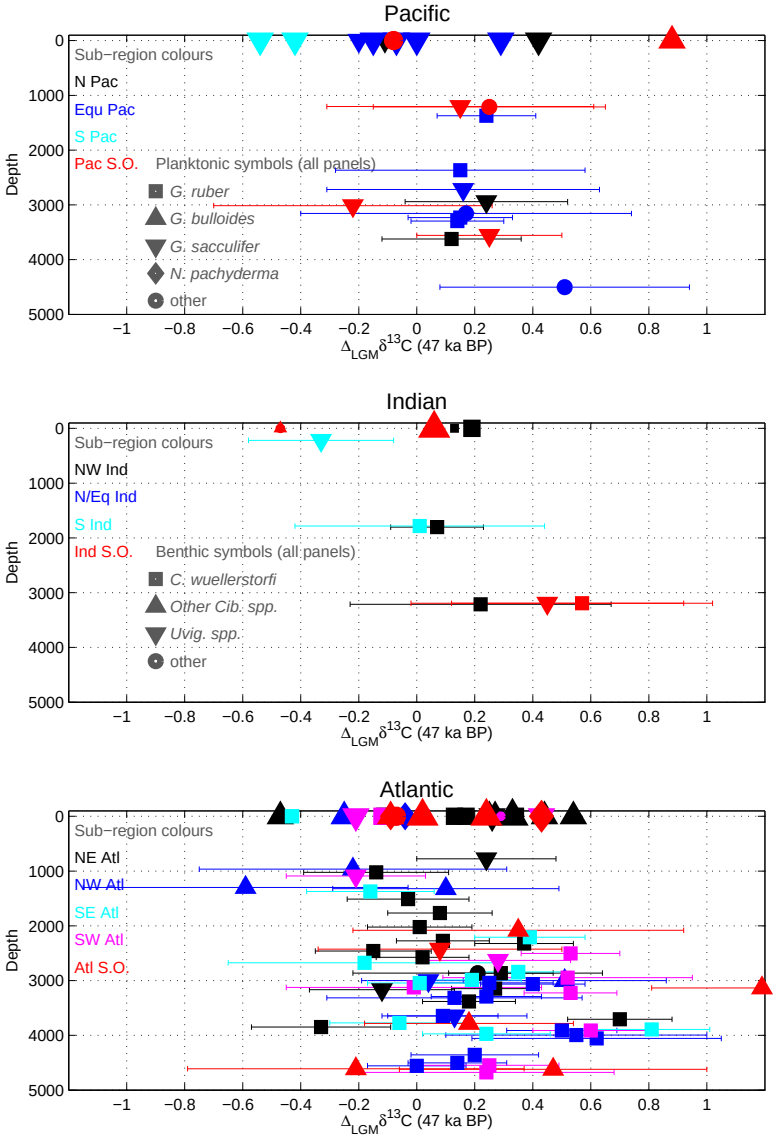

Fig. 12. 47 ka $\Delta_{LGM}\delta^{13}$C time-slice, with 2σ error bars on benthic data.

region to be distinguishable from random error, the apparent scatter in the data would exceed that predicted by the error bars. Since the scatter in the data in Figs. 10–14 are consistent with the quoted errors, we conclude that we have not underestimated the random error in the data. Furthermore, the estimated errors are likely to be too great to use the synthesis to reconstruct local changes in water mass boundaries, for which abundant well dated records from *C. wuellerstorfi* would be needed. The following discussion emphasises basin-scale changes in δ^{13}C that are coherent and statistically significant.

LGM δ^{13}C decreases with depth throughout the Atlantic Ocean (Fig. 10), with steep gradients existing at 1500–2500 m depth in the North Atlantic. Intermediate water is isotopically lighter in the South Atlantic than the North Atlantic, but these converge to approximately 0‰ in bottom waters (c.f. Bickert and Mackensen, 2003; Curry and Oppo, 2005). The very light values obtained in the Atlantic sector of the Southern Ocean may be influenced by a phytodetritus error (Mackensen et al., 1993), reflected in the large error bars. The data are not inconsistent with a decrease of δ^{13}C with depth in the Pacific and Indian Oceans comparable to that observed in the South Atlantic, but there are insufficient data to establish a statistically significant vertical trend in these basins. Absolute δ^{13}C derived from planktonic foraminifera is plotted for completeness, but these are subject to corrections for temperature and seawater chemistry. In Sect. 3.1.3, we described how Earth system model output fields could be

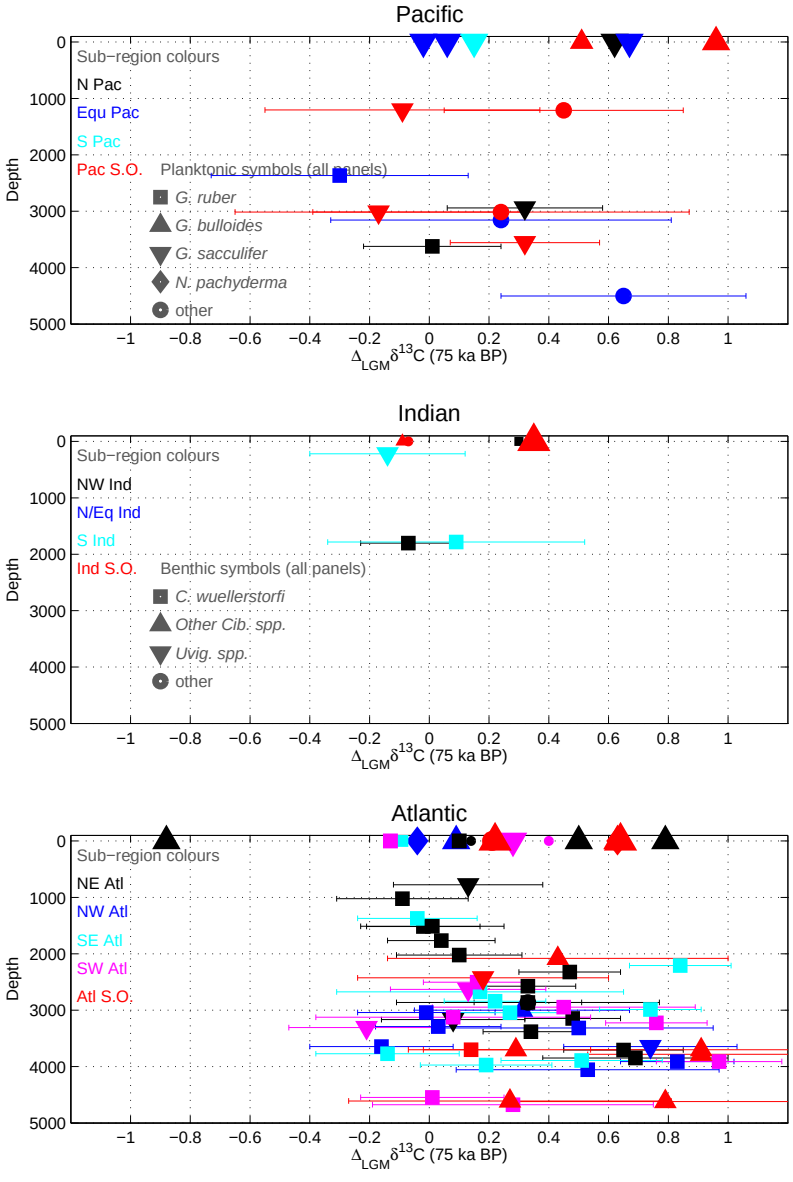

Fig. 13. 75 ka $\Delta_{LGM}\delta^{13}$C time-slice, with 2σ error bars on benthic data.

used to correct for these, whereas proxy data are not generally available over 150 kyr. Therefore, these adjustments are not included in Fig. 10, and although there is reasonable spatial coherence in the Pacific and Indian basins, we do not use absolute planktonic δ^{13}C in our interpretation.

The deep ocean is isotopically heavier during the 5 ka time-slice (Fig. 11), indicating a decrease in the vertical δ^{13}C gradient. Below 2500 m, mean Holocene $\Delta_{LGM}\delta^{13}$C is 0.44 ± 0.13‰ in Indo-Pacific Ocean records, 0.57 ± 0.10‰ in North Atlantic records and 0.60 ± 0.18‰ in the South Atlantic records (errors are double the standard error, approximately 95% confidence intervals; see also Fig. 7). It is cautioned that this calculation is based on the assumption that errors are random, and that quoted errors apply only to locations where observations exist. Uncertainties in mean $\Delta_{LGM}\delta^{13}$C within each ocean basin are much greater due to sampling biases. Nevertheless, the coherent signal observed throughout the deep ocean supports the hypothesis that the decrease in the vertical δ^{13}C gradient is principally a global signal. At intermediate depths, $\Delta_{LGM}\delta^{13}$C is typically indistinguishable from zero; however greater values of $\Delta_{LGM}\delta^{13}$C are obtained in the East Atlantic than the West Atlantic.

Although most individual $\Delta_{LGM}\delta^{13}$C observations cannot be distinguished from zero in the 47 ka time-slice (Fig. 12), the result that seawater was isotopically heavier

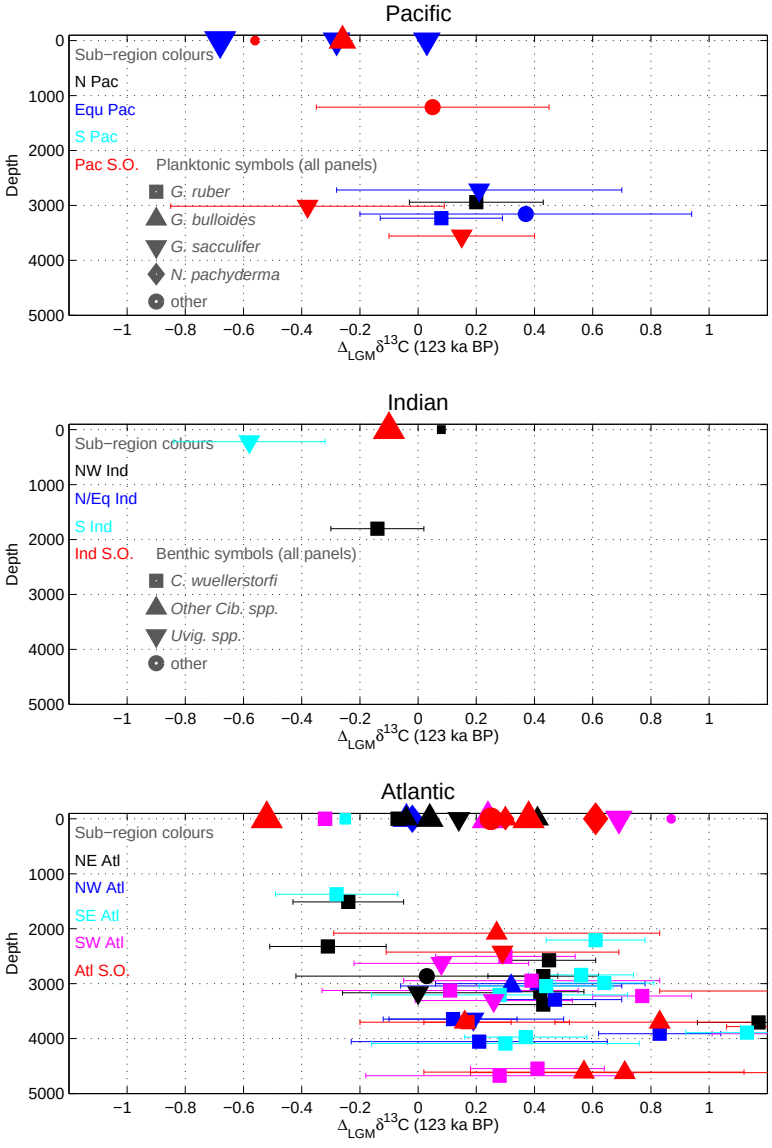

Fig. 14. 123 ka $\Delta_{LGM}\delta^{13}$C time-slice, with 2σ error bars on benthic data.

during MIS 3 than during the LGM is statistically significant (mean $\Delta_{LGM}\delta^{13}$C of 0.20 ± 0.06‰ in Atlantic records and 0.14 ± 0.11‰ in Indo-Pacific records). It is unclear whether this is a global signal, as four records suggest the presence of isotopically lighter waters in the intermediate-depth western Atlantic. There are no significant basin-scale differences between MIS 4 and LGM δ^{13}C distributions (Supplementary Fig. 1). However, the greatest decrease in ocean δ^{13}C occurred between MIS 5a and MIS 4. Below 2500 m in the 75 ka time-slice (Fig. 13), $\Delta_{LGM}\delta^{13}$C is 0.20 ± 0.13‰ in Indo-Pacific records, 0.40 ± 0.08‰ in North Atlantic records and 0.36 ± 0.11‰ in South Atlantic records. The last interglacial (MIS 5e; 123 ka; Fig. 14) is indistinguishable from MIS 5a in the Indo-Pacific (mean $\Delta_{LGM}\delta^{13}$C of 0.17 ± 0.11‰) or the North Atlantic (0.44 ± 0.11‰), but there is evidence that South Atlantic waters were isotopically heavier (mean $\Delta_{LGM}\delta^{13}$C of 0.53 ± 0.11‰) during the last interglacial than during MIS 5a, especially in bottom waters and Southern Ocean waters. Finally, an MIS 6 time-slice is provided in Supplementary Fig. 2, distinguishable from the LGM only by globally lower $\Delta_{LGM}\delta^{13}$C values (mean $\Delta_{LGM}\delta^{13}$C of -0.14 ± 0.10‰ in the Indo-Pacific, -0.15 ± 0.09‰ in the North Atlantic and -0.06 ± 0.09‰ in the South Atlantic).

4.4 Sensitivity to assumptions

In this section we examine the sensitivity of the data synthesis to the age model used and to assumptions made during the processing. All accompanying figures are provided in Supplementary Materials. Rather than propagating age error to an error in δ^{13}C, we have quoted an estimated 2σ error of 6–8 ka on output ages. To investigate the effect of this on $\Delta_{\mathrm{LGM}}\delta^{13}$C, we randomly add noise, sampled from the distributions plotted in Fig. 4, to each record. Supplementary Fig. 3 shows the effect of this noise on mean and standard deviation of $\Delta_{\mathrm{LGM}}\delta^{13}$C timeseries in each ocean basin. Changes are typically less than 0.1‰, but can be greater for regions with few records such as the Indian Ocean. The addition of such noise does not significantly reduce the coherence of the global or regional signals. We also investigated the effect of regionally tuning age models to nearby ^{14}C-derived age models. This was done by calculating the mean offset between our age estimate and previously published ^{14}C-derived age estimates in each ocean basin, and adjusting the age of all records in that basin to compensate for this. These adjustments were only made for the period 0–50 ka, and were less than 4 ka at all time-slices in all regions. Supplementary Fig. 4 shows that the effect on $\Delta_{\mathrm{LGM}}\delta^{13}$C is negligible. We conclude that, because age errors are typically small compared with the timescale of interest, our findings are robust to the choice of age model.

We did not apply a correction to $\Delta_{\mathrm{LGM}}\delta^{13}$C due to a time-variable phytodetritus effect, but instead added a random of error to records suspected of being influenced by this effect (flagged in Table 1). This leads to the hypothesis that the synthesis may be biased towards low δ^{13}C at the LGM (high $\Delta_{\mathrm{LGM}}\delta^{13}$C at other times) by such records. In Supplementary Fig. 5, we compare the mean and standard deviation of the entire synthesis with records from upwelling regions, and find that the amplitude and phase of variability is similar. A major exception is the Holocene $\Delta_{\mathrm{LGM}}\delta^{13}$C in the South Atlantic, which is approximately twice as great in phytodetritus-flagged records than in the entire synthesis, caused by five records from the Atlantic sector of the Antarctic Circumpolar Current. There is no similar amplification of $\Delta_{\mathrm{LGM}}\delta^{13}$C variability prior to the LGM, suggesting that any isotopically light microenvironment that formed at these sites persisted for most of a glacial cycle. Attributing a greater uncertainty to these records, as we have done, is preferable to removing them from the synthesis.

Finally, we test the hypothesis that the amplitude of the glacial cycle is underestimated in records with low sediment accumulation rates due to filtering of variability by bioturbation in sediment. Comparing the mean and standard deviation of the entire synthesis with records from sites with accumulation rates less than 3 cm/ka (Supplementary Fig. 6), we find no evidence for lower amplitude variability in records from sites with low accumulation rates; in intermediate depths, the amplitude of the MIS 6 to MIS 5e deglaciation is typically greater in these records. It is likely that filtering due to bioturbation is most important on timescales that have already been removed by the application of a 10 ka filter. Therefore, the synthesis already excludes any millennial timescale peak in δ^{13}C during interglacials, and this is not significantly exacerbated by the inclusion of records with low accumulation rates.

5 Discussion

We have presented benthic and planktonic δ^{13}C data over the last 150 ka. The reasonable global coverage within the synthesis depends on the inclusion of records from a variety of species, from high-productivity regions, and from regions with low sedimentation rates. This approach makes uncertainties an essential part of the data set; these were obtained using the entire dataset to estimate the additional error present in data from low resolution records and in less reliable species. Errors are smaller for estimates of $\Delta_{\mathrm{LGM}}\delta^{13}$C, the anomaly relative to the local LGM value, than for the absolute δ^{13}C because a large component of error is uniform within each record. $\Delta_{\mathrm{LGM}}\delta^{13}$C time-slices have the advantage over δ^{13}C time-slices as a modelling target that the latter target may favour states with errors that compensate for model error in the Holocene δ^{13}C distribution. We caution that, due to imprecision in the age-models, the data synthesis should not be used to examine inter-basin differences on timescales shorter than 10 ka. A final caveat is that much remains to be learnt about how changes in properties other than seawater δ^{13}C have influences the δ^{13}C record. Several such properties (notably temperature, $p\mathrm{CO}_2$ and carbonate ion concentration) are likely to change over a glacial cycle and introduce systematic errors to δ^{13}C change estimates (Sect. 3.1.3). This is of particular importance for data from planktonic foraminifera. We therefore caution that recorded variability in planktonic δ^{13}C may result from changes in ocean temperature and chemistry rather than in seawater δ^{13}C.

When comparing the LGM time-slice with previous studies, it should be noted that a uniform adjustment, representing estimated changes in biosphere carbon storage (Duplessy et al., 1988b), is frequently applied to δ^{13}C reconstructions, but is not applied in this study. We observe that isotopically light ($\delta^{13}\mathrm{C} < 0.5$‰) bottom waters penetrate north as far as the Iceland Basin, attributed to an expanded Antarctic overturning cell in the Atlantic Ocean relative to today (Bickert and Mackensen, 2003; Curry and Oppo, 2005). These studies focused on compiling benthic LGM time-slices for the Atlantic, and included cores, mostly from the West Atlantic, that are absent from our synthesis due to the age modelling constraint (Sect. 2.1). The addition of further West Atlantic cores reveals a zonal gradient in the LGM South Atlantic at intermediate depths, with isotopically lighter water of southern origin in the west (Curry

and Oppo, 2005), and isotopically heavier water of possible Mediterranean origin near the eastern boundary (Bickert and Mackensen, 2003). Our time-slice also excludes data from the Matsumoto and Lynch-Stieglitz (1999) compilation of southeast Pacific LGM data, where individual foraminer shells were interpreted as representing the LGM, based on δ^{18}O measurements. They obtained glacial δ^{13}C estimates of between -0.35 and -0.6‰ in the 2800-3800 m depth range. The result that the MIS 5e-MIS 6 δ^{13}C difference is analogous to the Holocene-LGM difference supports the findings of Duplessy and Shackleton (1985), who described an increase in δ^{13}C during deglaciation, although δ^{13}C was generally lower during MIS 5e compared with the Holocene (Duplessy et al., 1984). Govin et al. (2009) examined changes in δ^{13}C in 10 records from Atlantic and Antarctic source waters during glaciation. They found a two stage process, the decrease in Southern Ocean δ^{13}C occurring early during glacial inception, and predating changes in the North Atlantic. We find this result to be robust, and that moreover there is negligible net decrease in δ^{13}C outside the South Atlantic between the last interglacial and MIS 5a.

The data synthesis reveals a high degree of spatial coherence in δ^{13}C variability in the deep Atlantic and Pacific Oceans, with high values during temperature maxima and low values during temperature minima. The amplitude of variability in the Atlantic Ocean is approximately double that in the Pacific, suggesting that the δ^{13}C reservoir effect and ocean processes influencing deep Atlantic δ^{13}C act in phase and are of similar magnitude. The relative lack of variability in intermediate-depth North Atlantic δ^{13}C is consistent with a shoaling of ^{13}C-rich North Atlantic source waters during cold periods. The available data from outside the Atlantic Ocean also show less variability at intermediate depths. Atlantic δ^{13}C appears to be influenced by increases in δ^{13}C of the southern end-member during interglacials, but not during other temperature maxima. There is little evidence for basin-scale differences in δ^{13}C between MIS 1, 5a, 5c and 5e, or between MIS 2, 4 and 6 (except for the globally lower δ^{13}C values obtained during MIS 6), although individual records may show such differences. δ^{13}C at a given location may be interpreted in terms of highly local processes rather than large scale processes discussed in this paper. We therefore recommend that care be taken when using small numbers of records to infer changes in global phenomena. The similarity between MIS 5a and 5e suggests that the relationship between δ^{13}C and atmospheric pCO_2 over glacial cycles is complex. The major change in the δ^{13}C record occurs between MIS 5a and MIS 4, whereas much of the decrease in pCO_2 (and almost all of the decrease in Antarctic temperature) occurs between MIS 5e and MIS 5a (Fig. 7). Therefore, either the drawdown of pCO_2 during early glaciation occurred by a mechanism that does not decrease deep ocean δ^{13}C, or there was a compensating mechanism acting to increase deep ocean δ^{13}C without increasing pCO_2.

Constructing δ^{13}C inventories would be a valuable tool in estimating changes in carbon storage in the terrestrial biosphere and shelf sediments. Duplessy et al. (1988b) used Pacific data only to estimate the increase in the mean δ^{13}C of DIC in seawater between the LGM and the Holocene as +0.32‰. This yields a smaller change in carbon storage than is suggested by paleoecological reconstructions (Crowley, 1995; Peng et al., 1998), although the discrepancy would be partly explained if there was a lower proportion of isotopically light C_3 plants at the LGM than during the Holocene (François et al., 1999; Crucifix et al., 2005). Despite the coherence of the data presented here, we consider the coverage too incomplete to directly construct a time-series of δ^{13}C inventories. The principal gaps in benthic data suited to our age modelling method are in the Indian Ocean, intermediate depths in the Pacific Ocean, the Southern Ocean, and pycnocline depths throughout the global ocean. Nevertheless, there are sufficient data to tightly constrain the evolution of an Earth system model, and we propose data assimilation into such a model as a viable means to reconstruct biosphere carbon storage over the last glacial cycle.

Supplementary material related to this article is available online at: http://www.clim-past.net/6/645/2010/cp-6-645-2010-supplement.zip.

Acknowledgements. This study was funded by the NERC Quaternary QUEST programme. K. Oliver was supported by a Leverhulme Early Career Research Fellowship. We are grateful to the many researchers who have assisted us in compiling the data either through personal correspondence or by making records available via Pangaea or NGDC, for data obtained through the DELPHI project, and to two anonymous reviewers for improving the manuscript.

Edited by: T. Kiefer

References

Abrantes, F., Baas, J., Haflidason, H., Rasmussen, T. L., Klitgaard, D., Loncaric, N., and Gaspar, L.: Sediment fluxes along the northeastern European Margin: inferring hydrological changes between 20 and 8 kyr, Mar. Geol., 152, 7–23, 1998.

Anderson, D. M., Prell, W. L., and Barratt, N. J.: Estimates of sea surface temperature in the Coral Sea at the last glacial maximum, Paleoceanogr., 4, 615–627, 1989.

Arz, H. W., Pätzold, J., and Wefer, G.: The deglacial history of the western tropical Atlantic as inferred from high resolution stable isotope records off northeastern Brazil, Earth Planet. Sc. Lett., 167, 105–117, 1999.

Bassinot, F. C., Beaufort, L., Vincent, E., Labeyrie, L., Rostek, F., Müller, P. J., Quidelleur, X., and Lancelot, Y.: Coarse fraction fluctuations in pelagic carbonate sediments from the tropical Indian Ocean: A 1500-kyr record of carbonate dissolution, Paleoceanogr., 9, 579–600, 1994.

Bauch, H., Erlenkeuser, H., Spielhagen, R. F., Struck, U., Matthiessen, J., Thiede, J., and Heinemeier, J.: A multiproxy reconstruction of the evolution of deep and surface waters in the subarctic Nordic seas over the last 30 000 years, Quaternary Sci. Rev., 20, 659–678, 2001.

Bemis, B. E., Spero, H. J., Lea, D. W., and Bijma, J.: Temperature influence on the carbon isotopic composition of *Globigerina bulloides* and *Orbulina universa* (planktonic foraminifera), Mar. Micropaleontol., 38, 213–228, 2000.

Berger, W. H., Killingley, J. S., and Vincent, E.: Stable isotopes in deep-sea carbonates: box core ERDC-92 west equatorial Pacific, Oceanol. Acta, 1, 203–216, 1978.

Beveridge, N. A. S., Elderfield, H., and Shackleton, N. J.: Deep thermohaline circulation in the low-latitude Atlantic during the last glacial, Paleoceanogr., 10, 643–660, 1995.

Bickert, T. and Mackensen, A.: Last Glacial to Holocene Changes in South Atlantic deep water circulation, in: The South Atlantic in the late Quaternary: Reconstruction of material budgets and current systems, edited by Wefer, G., Mulitza, S., and Ratmeyer, V., 671–695, Springer-Verlag Berlin Heidelberg New York Tokyo, 2003.

Bickert, T. and Wefer, G.: Late Quaternary deep water circulation in the South Atlantic: Reconstruction from carbonate dissolution and benthic stable isotopes, in: Wefer et al. (1996b), 599–620, 1996.

Bickert, T. and Wefer, G.: South Atlantic and benthic foraminifer δ^{13}C-deviations: Implications for reconstructing the Late Quaternary deep-water circulation, Deep-Sea Res. I, 46, 437–452, 1999.

Bickert, T., Curry, W. B., and Wefer, G.: Late Pliocene to Holocene (2.60 Ma) western equatorial Atlantic deep-water circulation: Inferences from stable isotopes, Proc. Ocean Drill. Program Sci. Results, 154, 239–253, 1997.

Boyle, E.: Vertical oceanic nutrient fractionation and glacial/interglacial CO_2 cycles, Nature, 331, 55–56, 1988.

Broecker, W. S.: Ocean chemistry during glacial time, Geochem. Cosmochim. Acta, 46, 1689–1705, 1982a.

Broecker, W. S.: Tracers in the Sea, Eldigio Press, New York, 690 pp., 1982b.

Brovkin, V., Ganapolski, A., Archer, D., and Rahmstorf, S.: Lowering of glacial atmospheric CO_2 in response to changes in oceanic circulation and marine biogeochemistry, Paleoceanogr., 22, PA4202, doi:10.1029/2006PA001380, 2007.

Cannariato, K. G. and Ravelo, A. C.: Pliocene-Pleistocene evolution of eastern tropical Pacific surface water circulation and thermocline depth, Paleoceanogr., 12, 805–820, 1997.

Carter, L., Manighetti, B., Ganssen, G., and Northcote, L.: Southwest Pacific modulation of abrupt climate change during the Antarctic Cold ReversalYounger Dryas, Palaeogeogr. Palaeoclimatol. Palaeoecol., 260, 284–298, 2008.

Chapman, M. R. and Shackleton, N. J.: Global ice-volume fluctuations, North Atlantic ice-rafting events, and deep-ocean circulation changes between 130 and 70 ka, Geology, 27, 795–798, 1999.

Cortijo, E.: Stable isotope analysis on sediment core SU90-39, PANGAEA, doi:10.1594/PANGAEA.106761, 2003.

Crowley, T. J.: Ice age terrestrial carbon changes revisited, Global Biogeochem. Cy., 9, 377–389, 1995.

Crucifix, M., Betts, R. A., and Hewitt, C. D.: Pre-industrial-potential and Last Glacial Maximum global vegetation simulated with a coupled climate-biosphere model: Diagnosis of bioclimatic relationships, Global Planet. Change, 45, 295–312, 2005.

Curry, W. B. and Oppo, D. W.: Synchronous, high-frequency oscillations in tropical sea surface temperatures and North Atlantic Deep Water productivity during the last glacial cycle, Paleoceanogr., 12, 1–14, 1997.

Curry, W. B. and Oppo, D. W.: Glacial water mass geometry and the distribution of δ^{13}C of ΣCO2 in the western Atlantic Ocean, Paleoceanogr., 20, PA1017, doi:10.1029/2004PA001021, 2005.

Curry, W. B., Duplessy, J.-C., Labeyrie, L., and Shackleton, N. J.: Changes in the distribution of d13C of deep water ΣCO2 between the last glaciation and the Holocene, Paleoceanogr., 3, 317–341, 1988.

Dorschel, B., Hebbeln, D., Rggeberg, A., Dullo, W.-C., and Freiwald, A.: Growth and Erosion of a Cold-Water Coral Covered Carbonate Mound in the Northeast Atlantic during the Late Pleistocene and Holocene, Earth Planet. Sc. Lett., 233, 33–44, 2005.

Duplessy, J.-C.: Quaternary paleoceanography: unpublished stable isotope records. IGBP PAGES/World Data Center for Paleoclimatology Data Contribution Series #1996-035., NOAA/NGDC Paleoclimatology Program, Boulder, Colorado, USA, 1996.

Duplessy, J. C. and Shackleton, N.: Response of global deep-water circulation to Earth's climatic change 135,000–107,000 years ago, Nature, 316, 500–507, 1985.

Duplessy, J. C., Bé, A. W. H., and Blanc, P. L.: Oxygen and carbon isotopic composition and biogeographic distribution of planktonic foraminifera in the Indian Ocean, Palaeogeogr. Palaeoclimatol. Palaeoecol., 33, 9–46, 1981a.

Duplessy, J. C., Blanc, P. L., and Bé, A. W. H.: Oxygen-18 Enrichment of Planktonic Foraminifera Due to Gametogenic Calcification Below the Euphotic Zone, Science, 213, 1247–1250, 1981b.

Duplessy, J. C., Shackleton, N. J., Matthews, R. K., Prell, W., Ruddiman, W. F., Caralp, M., and Hendy, C. H.: 13C record of benthic foraminifera in the last interglacial ocean: Implications for the carbon cycle and the global deep water circulation, Quat. Res., 21, 225–243, 1984.

Duplessy, J. C., Labeyrie, L., and Blanc, P. L.: Norwegian Sea Deep Water variations over the last climatic cycle: Paleoceanographical implications, in: Long and short term variability of climate, edited by Wanner, H. and Siegenthaler, U., 83–116, Springer, Heidelberg, 1988a.

Duplessy, J. C., Shackleton, N. J., Fairbanks, R. G., Labeyrie, L., Oppo, D., and kallel, N.: Deepwater source variations during the last climatic cycle and their impact on the global deepwater circulation, Paleoceanogr., 3, 343–360, 1988b.

Duplessy, J.-C., Labeyrie, L., Arnold, M., Paterne, M., Duprat, J., and van Weering, T. C. E.: Changes in surface salinity of the North Atlantic ocean during the last deglaciation, Nature, 358, 485–488, 1992.

Dürkop, A., Hale, W., Mulitza, S., PŁtzold, J., and Wefer, G.: Late Quaternary variations of sea surface salinity and temperature in the western tropical Atlantic: Evidence from d18O of Globigerinoides sacculifer, Paleoceanogr., 12, 764–772, 1997.

Elderfield, H., Vautravers, M., and Cooper, M.: The relationship between shell size and Mg/Ca, Sr/Ca, d18O and d13C of species of planktonic foraminifera, Geochem. Geophys. Geosyst., 3, doi:10.1029/2001GC000194, 2001GC000194, 2002.

Enting, I.: On the use of smoothing splines to filter CO_2 data, J. Geophys. Res., 92, 10977–10984, 1987.

Fischer, G., Kalberer, M., Donner, B., and Wefer, G.: Stable isotopes of pteropod shells as recorders of sub-surface water conditions: Comparison to the record of *G. ruber* and to measured values, in: Use of Proxies in Paleoceanography, edited by: Fischer, G. and Wefer, G., Examples from the South Atlantic, Springer-Verlag, 191–206, 1999.

François, L. M., Goddéris, Y., Warnant, P., Ramstein, G., de Noblet, N., and Lorenz, S.: Carbon stocks and isotopic budgets of the terrestrial biosphere at mid-Holocene and last glacial maximum times, Chem. Geol., 159, 163–189, 1999.

Freudenthal, T., Meggers, H., Henderiks, J., Kuhlmann, H., Moreno, A., and Wefer, G.: Upwelling intensity and filament activity off Morocco during the last 250,000 years, Deep Sea Res. II, 49, 3655–3674, 2002.

Gorbarenko, S. A. and Southon, J. R.: Detailed Japan Sea paleoceanography during last 25Kyr: constraints from AMS dating and d18O of planktonic foraminifera, Palaeogeogr. Palaeoclimatol. Palaeoecol., 156, 177–193, 2000.

Govin, A., Michel, E., Labeyrie, L., Waelbroeck, C., Dewilde, F., and Jansen, E.: Evidence for northward expansion of Antarctic Bottom Water mass in the Southern Ocean during the last glacial inception, Paleoceanogr., 14, PA1202, doi:10.1029/2008PA001603, 2009.

Hale, W. and Pflaumann, U.: Sea-surface Temperature Estimations using a Modern Analog Technique with Foraminiferal Assemblages from Western Atlantic Quaternary Sediments, in: Use of Proxies in Paleoceanography, edited by: Fischer, G. and Wefer, G., Examples from the South Atlantic, Springer-Verlag, 69–90, 1999.

Hodell, D. A., Venz, K. A., Charles, C. D., and Ninnemann, U. S.: Pleistocene vertical carbon isotope and carbonate gradients in the South Atlantic sector of the Southern Ocean, Geochem. Geophy. Geosy., 4, doi:10.1029/2002GC000367, 2003.

Holbourn, A. E., Kuhnt, W., and James, N.: Late Pleistocene bryozoan reef mounds of the Great Australian Bight: isotope stratigraphy and benthic foraminiferal record, Paleoceanogr., 17, doi:10.1029/2001PA000643, 2002.

Hoogakker, B. A. A. Rohling, E. J., Palmer, M. R., Tyrrell, T., and Rothwell, R. G.: Underlying causes for long-term global ocean δ^{13}C fluctuations over the last 1.20 Myr, Earth Planet. Sc. Lett., 248, 15–29, 2006.

Hoogakker, B. A. A., Elderfield, H., Oliver, K. I. C., and Crowhurst, S.: Benthic foraminiferal isotope offsets over the last glacial-interglacial cycle, Paleoceanogr., in press, doi:10.1029/2009PA001870, 2010.

Howard, W. R. and Prell, W. L.: Late Quaternary carbonate production and preservation in the Southern Ocean: implications for oceanic and atmospheric carbon cycling, Paleoceanogr., 9, 453–482, 1994.

Hüls, M.: Stable isotope analysis on sediment core M35003-4, PANGAEA, 29, doi:10.1594/PANGAEA.55754, 1999.

Imbrie, J., McIntyre, A., and Mix, A. C.: Composite stable isotope data (adjusted) for sediment core RC12-294 (specmap.002), PANGAEA, doi:10.1594/PANGAEA.52117, 1997.

Jung, S. J. A.: Stable isotope analysis of foraminifera from sediment core SO82_5-2, PANGAEA, doi:10.1594/PANGAEA.201812, 2004.

Jung, S. J. A. and Sarnthein, M.: Stable isotope data of sediment cores GIK23419-8, PANGAEA, doi:10.1594/PANGAEA.112916, 2003a.

Jung, S. J. A. and Sarnthein, M.: Stable isotope data of sediment cores GIK23414-9, PANGAEA, doi:10.1594/PANGAEA.112911, 2003b.

Jung, S. J. A. and Sarnthein, M.: Stable isotope data of sediment cores GIK23415-9, PANGAEA, doi:10.1594/PANGAEA.112912, 2003c.

Jung, S. J. A. and Sarnthein, M.: Stable isotope data of sediment cores GIK23418-8, PANGAEA, doi:10.1594/PANGAEA.112915, 2003d.

Jung, S. J. A. and Sarnthein, M.: Stable isotope data of sediment cores GIK23417-1, PANGAEA, doi:10.1594/PANGAEA.112914, 2003e.

Jung, S. J. A. and Sarnthein, M.: Stable isotope analysis of foraminifera from sediment cores GIK17049-6, PANGAEA, doi:10.1594/PANGAEA.112908, 2004a.

Jung, S. J. A. and Sarnthein, M.: Stable isotope data of core GIK23416-4, PANGAEA, doi:10.1594/PANGAEA.136423, 2004b.

Jung, S. J. A., Kroon, D., Ganssen, G., Peeters, F., and Ganeshram, R.: Enhanced Arabian Sea intermediate water flow during glacial North Atlantic cold phases, Earth Planet. Sc. Lett., 280, 220–228, 2009.

Kawamura, H., Holbourn, A. E., and Kuhnt, W.: Climate variability and land-ocean interactions in the Indo Pacific Warm Pool: A 460-ka palynological and organic geochemical record from the Timor Sea, Mar. Micropaleontol., 59, 1–14, 2006.

Kawamura, K., Parrenin, F., Lisiecki, L., Uemura, R., Vimeux, F., Severinghaus, P., Hutterli, M. A., Nakazawa, T., Aoki, S., Jouzel, J., Raymo, M. E., Matsumoto, K., Nakata, H., Motoyama, H., Fujita, S., Goto-Azuma, K., Fujii, Y., and Watanabe, O.: Northern Hemisphere forcing of climatic cycles in Antarctica over the past 360,000 years, Nature, 448, 912–917, 2007.

Keigwin, L. D.: Radiocarbon and stable isotope constraints on Last Glacial Maximum and Younger Dryas ventilation in the western North Atlantic, Paleoceanogr., 19, PA4012, doi:10.1029/2004PA001029, 2004.

Kohfeld, K. E., Anderson, R. F., and Lynch-Stieglitz, J.: Carbon isotopic disequilibrium in polar planktonic foraminifera and its impact on modern and Last Glacial Maximum reconstructions, Paleoceanogr., 15, 53–64, 2000.

Kroopnick, P.: The distribution of ^{13}C of TCO_2 in the world oceans, Deep Sea Res., 32, 57–84, 1985.

Labeyrie, L.: Quaternary paleoceanography: unpublished stable isotope records. IGBP PAGES/World Data Center for Paleoclimatology Data Contribution Series #1996-036, NOAA/NGDC Paleoclimatology Program, Boulder, Colorado, USA, 1996.

Labeyrie, L.: Stable isotope analysis on foraminifera from sediment core MD88-770, PANGAEA, doi:10.1594/PANGAEA.52728, 1998.

Labeyrie, L., Vidal, L., Cortijo, E., Paterne, M., Arnold, M., Duplessy, J.-C., Vautravers, M., Labracherie, M., Duprat, J., Turon, J. L., Grousset, F., and Van Weering, T.: Surface and deep hydrology of the Northern Atlantic Ocean during the last 150000 years, Phil. Trans. Royal Soc. London, B, 348, 255–264, 1995.

Labeyrie, L. D., Waelbroeck, C., Cortijo, E., Michel, E., and Duplessy, J.-C.: Changes in deep water hydrology during the Last

Deglaciation, C. R. Geoscience, 337, 919–927, 2005.

Lea, D. W., Pak, D. K., and Spero, H. J.: Climate impact of late Quaternary, equatorial Pacific sea surface temperature variations, Science, 289, 1719–1724, 2000.

Lowry, R. K., Machin, P., and Cramer, R. N.: BOFS North Atlantic Data Set. Oceanographic data collected during the North Atlantic cruises of the NERC Biogeochemical Ocean Flux Study (1989–1991): a UK contribution of JGOFS, Natural Environmental Research Council, British Oceanographic Data Centre, Merseyside, UK, 1994.

Lynch-Stieglitz, J., Curry, W., and Oppo, D.: Meridional overturning circulation in the South Atlantic at the last glacial maximum, Geochem. Geophys. Geosyst., 7, doi:10.1029/2005GC001226, 2006.

Lynch-Stieglitz, J., Adkins, J. F., Curry, W. B., Dokken, T., Hall, I. R., Herguera, J. C., Hirschi, J. J.-M., Ivanova, E., Kissell, C., Marchal, O., Marchitto, T. M., McCave, I. N., McManus, J. F., Mulitza, S., Ninnemann, U. S., Yu, E.-F., and Zahn, R.: Atlantic overturning circulation during the last glacial maximum, Science, 316, 66–69, 2007.

Mackensen, A., Hubberten, H. W., Bickert, T., Fischer, G., and Fütterer, D. K.: δ^{13}C in benthic foraminiferal tests of *Fontbotia wuellerstorfi* (Schwager) relative to δ^{13}C of dissolved inorganic carbon in Southern Ocean deep water: implications for glacial ocean circulation models, Paleoceanogr., 8, 587–610, 1993.

Mackensen, A., Grobe, H., Hubberten, H. W., and Kuhn, G.: Benthic foraminiferal assemblages and the d13C-signal in the Atlantic sector of the Southern Ocean: Glacial-to-interglacial contrasts, in: Carbon cycling in the glacial ocean: Constraints on the ocean's role in global change, edited by: Zahn, R., Kaminski, M., Labeyrie, L., and Pedersen, T., NATO ASI series, Springer, Berlin, I 17, 105–144, 1994.

Mackensen, A., Rudolph, M., and Kuhn, G.: Late Pleistocene deepwater circulation in the subantarctic eastern Atlantic, Global Planet Change, 30, 197–229, 2001.

Marchitto, T. M. and Broecker, W. S.: Deep water mass geometry in the glacial Atlantic Ocean: A review of constraints from the paleonutrient proxy Cd/Ca, Geochem. Geophys. Geosys., 7, 10.1029/2006GC001323, 2006.

MARGO Project Members: Constraints on the magnitude and patterns of ocean cooling at the Last Glacial Maximum, Nature Geosci., 2, 127–132, 2009.

Martinson, D. G., Pisias, N. G., Hays, J. D., Imbrie, J. D., Moore, T. C., and Shackleton, N. J.: Age Dating and the orbital theory of the ice ages: development of a high-resolution 0 to 300,000-year chronostratigraphy, Quaternary Res., 27, 1–29, 1987.

Matsumoto, K. and Lynch-Stieglitz, J.: Similar glacial and Holocene deep water circulation inferred from southeast Pacific benthic foraminiferal carbon isotope composition, Paleoceanogr., 14, 149–163, 1999.

McCave, I. N., Carter, L., and Hall, I. R.: Glacial-interglacial changes in water mass structure and flow in the SW Pacific, Quaternay Sci. Rev., 27, 1886–1908, doi:10.1016/j.quascirev.2008.07.010, 2008.

McConnaughey, T. A., Burdett, J., Whelan, J. F., and Paull, C. K.: Carbon isotopes in biological carbonates: respiration and photosynthesis, Geochim. Cosmochim. Acta, 62, 611–622, 1997.

McIntyre, A., Ruddiman, W. F., karlin, K., and Mix, A. C.: Surface water response of the Equatorial Atlantic Ocean to orbital forcing, Paleoceanogr., 4, 19–55, 1989.

Mix, A. C., Pisias, N. G., Zahn, R., Rugh, W., Lopez, C., and Nelson, K.: Carbon 13 in Pacific deep and intermediate waters, 0–370 ka: implications for ocean circulation and Pleistocene CO_2, Paleoceanogr., 6, 205–226, 1991.

Mix, A. C., Bard, E., and Schneider, R.: Environmental processes of the ice age: land, oceans, glaciers (EPILOG), Quaternary Sci. Rev., 20, 627–657, 2001.

Mollenhauer, G., Schneider, R. R., Müller, P. J., Spiess, V., and Wefer, G.: Glacial/interglacial variability in the Benguela upwelling system: Spatial distribution and budgets of organic carbon accumulation, Global Biogeochem. Cy., 16, doi:10.1029/2001GB001488, 2002.

Morley, J. J., Heusser, L. E., and Shackleton, N. J.: Late Pleistocene/Holocene radiolarian and pollen records from sediments in the sea of Okhotsk, Paleoceanogr., 6, 121–131, 1991.

Mulitza, S.: Stable isotopes of sediment core GeoB1523-2, PANGAEA, doi:10.1594/PANGAEA.54618, 1998.

Nørgaard-Pedersen, N., Spielhagen, R. F., Thiede, J., and kassens, H.: Central Arctic surface ocean environment during the past 80,000 years, Paleoceanogr., 13, 193–204, 1998.

Oppo, D. W. and Fairbanks, F. G.: Variability in the deep and intermediate water circulation of the Atlantic Ocean during the past 25000 years: Northern Hemisphere modulation of the Southern Ocean, Earth Planet. Sc. Lett., 86, 1–15, 1987.

Oppo, D. W. and Fairbanks, R. G.: Carbon isotopic comparison of tropical surface water during the past 22,000 year, Paleoceanogr., 4, 333–351, 1989.

Oppo, D. W. and Lehmann, S. J.: Suborbital timescale variability of North Atlantic Deep Water during the past 200,000 years, Paleoceanogr., 10, 901–910, 1995.

Oppo, D. W., Fairbanks, R. G., Gordon, A. L., and Shackleton, N. J.: Late Pleistocene Southern Ocean d13C variability, Paleoceanogr., 5, 43–54, 1990.

Oppo, D. W., McManus, J. F., and Cullen, J. L.: Palaeooceanography: Deepwater variability in the Holocene epoch, Nature, 422, 277, 2003.

Pahnke, K., Zahn, R., Elderfield, H., and Schulz, M.: 340,000-Year centennial-scale marine record of southern hemisphere climatic oscillation, Science, 301, 948–952, 2003.

Patrick, A. and Thunell, R. C.: Tropical Pacific sea surface temperatures and upper water column thermal structure during the last glacial maximum, Paleoceanogr., 12, 649–657, 1997.

Peng, C. H., Guiot, J., and Van Campo, E.: Estimating changes in terrestrial vegetation and carbon storage: using paleoecological data and models, Quaternary Sci. Rev., 17, 719–735, 1998.

Pierre, C., Saliege, J. F., Urrutiaguer, M. J., and Giraudeau, J.: Stable isotope record of the last 500 k.y. at Site 1087 (Southern Cape Basin), Proc. Ocean Drill. Program Sci. Results, 175, 2001.

Prell, W. L., Hutson, W. H., Williams, D. F., Bé, A. W. H., Geitzenauer, K., and Molfino, B.: Surface circulation of the Indian Ocean during the last glacial maximum, approximately 18,000 yr B.P., Quaternary Res., 14, 309–336, 1980.

Rau, A., Roger, J., Lutjeharms, J., Giraudeau, J., Lee-Thorp, J., Chen, M.-T., and Waelbroeck, C.: A 450-kyr record of hydrological conditions on the western Agulhas Bank Slope, south of Africa, Marine Geol., 180, 183–201, doi:10.1016/S0025–3227(01)00213–4, 2002.

Richter, T.: Stable isotope data of sediment core GEOFAR KF09,

PANGAEA, doi:10.1594/PANGAEA.66316, 2001.
Rickaby, R. E. M. and Elderfield, H.: Planktonic foraminiferal Cd/Ca: Paleonutrients or paleotemperature?, Paleoceanogr., 14, 293–303, 1999.
Rickaby, R. E. M., Elderfield, H., Roberts, N., Hillenbrand, C.-D., and Mackensen, A.: Evidence for elevated alkalinity in the glacial Southern Ocean, Paleoceanogr., in press, 2009.
Ridgwell, A., Hargreaves, J. C., Edwards, N. R., Annan, J. D., Lenton, T. M., Marsh, R., Yool, A., and Watson, A.: Marine geochemical data assimilation in an efficient Earth System Model of global biogeochemical cycling, Biogeosciences, 4, 87–104, doi:10.5194/bg-4-87-2007, 2007.
Ruddiman, W. F. and CLIMAP Project Members: Stable isotope data of the 120 k time slice, PANGAEA, doi:10.1594/PANGAEA.51932, 1997.
Rüggeberg, A., Dorschel, B., Dullo, W-C., and Hebbeln, D.: Stable isotope ratios of benthic foraminifera from sediment core GeoB6719-1, PANGAEA, doi:10.1594/PANGAEA.134555, 2005.
Russon, T., Elliot, M., Kissel, C., Cabioch, G., De Deckker, P., and Corrège, T.: Middle-late Pleistocene deep water circulation in the southwest subtropical Pacific, Paleoceanogr., 24, doi:10.1029/2009PA001755, 2009.
Sarnthein, M. and Voelker, A.: Stable isotope analysis on sediment core GIK23071-3, PANGAEA, 9, doi:10.1594/PANGAEA.58000, 2001.
Sarnthein, M., Winn, K., Jung, S. J. A., Duplessy, J.-C., Labeyrie, L., Erlenkeuser, H., and Ganssen, G. M.: Changes in east Atlantic deepwater circulation over the last 30,000 years: Eight time slice reconstructions, Paleoceanography, 9, 209–267, 1994.
Schmiedl, G. and Mackensen, A.: Late Quaternary paleoproductivity and deep water circulation in the eastern South Altantic Ocean: Evidence from benthic foraminifera, Palaeogeog., Palaeoclim., Palaeoecol., 130, 43–80, 1997.
Schmiedl, G. and Mackensen, A.: Stable oxygen isotope records of different benthic foraminiferal species of core GeoB3004-1 from the western Arabian Sea, PANGAEA, doi:10.1594/PANGAEA.548185, 2006.
Schulz, H., von Rad, U., and Erlenkeuser, H.: Correlation between Arabian Sea and Greenland climate oscillations of the past 110,000 years, Nature, 393, 54–57, 1998.
Shackleton, N. J.: Carbon-13 in Uvigerina: tropical rainforest history and the equatorial Pacific carbonate dissolution cycles, in: The fate of fossil fuel CO_2 in the oceans, edited by: Anderson, N. R. and Malahoff, A., 401–423, Plenum Press, 1977.
Shackleton, N. J. and Hall, M. A.: Oxygen and carbon isotope stratigraphy of Deep Sea Drilling Project Hole 552A: Plio-Pleistocene glacial history, Initial Rep. of the Deep Sea Drill. Proj., 81, 599–610, 1984.
Shackleton, N. J., Hall, M. A., Line, J., and Cang, S.: Carbon isotope data in core V19-30 confirm reduced carbon dioxide concentration in the ice age atmosphere, Nature, 306, 319–322, 1983.
Shackleton, N. J., Le, J., Mix, A., and Hall, M. A.: Carbon isotope records from Pacific surface waters and atmospheric carbon dioxide, Quaternary Sci. Rev., 11, 387–400, 1992.
Shackleton, N. J., Hall, M. A., and Pate, D.: Pliocene stable isotope stratigraphy of Site 846, Proc. Ocean Drill. Program Sci. Results, 138, 337–355, 1995.
Shackleton, N. J., Hall, M. A., and Vincent, E.: Phase relationships between millennial-scale events 64,000–24,000 years ago, Paleoceanogr., 15, 565–569, doi:10.1029/2000PA000513, 2000.
Sikes, E. L. and Keigwin, L. D.: Equatorial Atlantic sea surface temperature for the last 30 kyr: A comparison of Uk37, delO18 and foraminiferal assemblage temperature estimates, Paleoceanogr., 9, 31–45, 1994.
Silverman, B. W.: Aspects of the spline smoothing approach to non-parametric regression curve fitting, J. Royal Stat. Soc. Ser. B, 47, 1–52, 1985.
Sirocko, F.: Sedimentology on core IOE105KK, PANGAEA, doi:10.1594/PANGAEA.77634, 2002.
Sirocko, F., Sarnthein, M., Erlenkeuser, H., Lange, H., Arnold, M., and Duplessy, J.-C.: Century-Scale events in monsoonal climate over the past 24,000 years, Nature, 364, 322–324, 1993.
Sirocko, F., Garbe-Schönberg, D., and Devey, C. W.: Processes controlling trace element geochemistry of Arabian Sea sediments during the last 25,000 years, Global Planet. Change, 26, 217–303, 2000.
Skinner, L. C. and Shackleton, N. J.: An Atlantic lead over Pacific deep-water change across Termination I: implications for the application of the marine isotope stage stratigraphy, Quaternary Sci. Rev., 24, 571–580, 2005.
Slowey, N. C. and Curry, W. B.: Glacial-interglacial differences in circulation and carbon cycling within the upper western Atlantic, Paleoceanogr., 10, 715–732, 1995.
Spero, H. J. and Lea, D. W.: Intraspecific stable isotope variability in the planktonic foraminifera *Globigerinoides sacculifer*: results from laboratory experiments, Mar. Micropaleontol., 22, 221–234, 1993.
Spero, H. J. and Lea, D. W.: Experimental determination of stable isotope variability in *Globigerina bulloides*: Implications for paleoceanographuc reconstructions, Mar. Micropaleontol., 28, 231–246, 1996.
Spero, H. J., Bijma, J., Lea, D. W., and Bemis, B. E.: Effect of seawater carbonate concentration on foraminiferal carbon and oxygen isotopes, Nature, 390, 497–500, 1997.
Thunell, R. C., Qingmin, M., Calvert, S. E., and Pedersen, T. F.: Glacial-Holocene biogenic sedimentation Patterns in the South China Sea: productivity variations and surface water pCO2, Paleoceanogr., 7, 143–162, 1992.
Tian, J., Wang, P. X., Chen, X. R., and Li, Q. Y.: Astronomically tuned Plio-Pleistocene benthic d18O records from South China Sea and Atlantic-Pacific comparison, Earth Planet. Sc. Lett., 203, 1015–1029, 2002.
Venz, K. A., Hodell, D. A., Stanton, C., and Warnke, D. A.: A 1.0 Myr record of glacial North Atlantic intermediate water variability from ODP site 982 in the northeast Atlantic, Paleoceanogr., 14, 42–52, 1999.
Voelker, A.: Stable isotopes on Cibicidoides pachyderma of sediment core MD99-2339, PANGAEA, doi:10.1594/PANGAEA.465028, 2006.
Weaver, P. P. E., Carter, L., and Neil., H. L.: Response of surface water masses and circulation to late Quaternary climate change east of New Zealand, Paleoceanogr., 13, 70–83, 1998.
Wefer, G., Berger, W. H., Bickert, T., Donner, B., Fischer, G., Kemle-von Mücke, S., Pätzold, J., Meinecke, G., Mller, P. J., Mulitza, S., Niebler, H.-S., Schmidt, H., Schneider, R., and Segl, M.: Late Quaternary surface circulation of the South Atlantic:

The stable isotope record and implications for heat transport and productivity, in: Wefer et al. (1996b), 461–502, 1996a.

Wefer, G., Berger, W. H., Siedler, G., and Webb, D., eds.: The South Atlantic in the late Quaternary: Present and Past Circulation, Springer-Verlag, Berlin, 1996b.

Weinelt, M. and Sarnthein, M.: Stable isotope analysis on sediment core GIK11944-2, PANGAEA, 29, doi:10.1594/PANGAEA.97 104, 2003.

Zabel, M., Bickert, T., Dittert, L., and Haese, R. R.: Significance of the sedimentary Al:Ti ratio as an indicator for variations in the circulation patterns of the equatorial North Atlantic, Paleoceanogr., 14, 789–799, 1999.

Zahn, R., Winn, K., and Sarnthein, M.: Benthic foraminiferal d13C and accumulation rates of organic carbon: Uvigerina peregrina group and Cibicidoides wuellerstorfi, Paleoceanogr., 1, 27–42, 1986.

Zahn-Knoll, R. and Sarnthein, M.: Stable isotope analysis on sediment core GIK15669-1, PANGAEA, doi:10.1594/PANGAEA.106214, 2003a.

Zahn-Knoll, R. and Sarnthein, M.: Stable isotope analysis on sediment core GIK15637-1, PANGAEA, doi:10.1594/PANGAEA.106213, 2003b.

Zhao, M., Beveridge, N. A. S., Shackleton, N. J., Sarnthein, M., and Eglinton, G.: Molecular stratigraphy of cores off northwest Africa: Sea surface temperature history over the last 80 ka, Paleoceanogr., 10, 661–675, 1995.